Degradable Piezoelectric Biomaterials for Wearable and Implantable Bioelectronics

Jun Li, **Yin Long**, **Fan Yang**, **Xudong Wang**

Department of Materials Science and Engineering, University of Wisconsin-Madison, Madison, Wisconsin 53706, USA

Abstract

Current bioelectronics are facing a paradigm shift from old-fashioned unrecyclable materials to green and degradable functional materials with desired biocompatibility. As an essential electromechanical coupling component in many bioelectronics, new piezoelectric materials are being developed with biodegradability, as well as desired mechanical and electromechanical properties for the next generation implantable and wearable bioelectronics. In this review, we provide an overview of the major advancements in biodegradable piezoelectric materials. Different natural (such as peptide, amino acids, proteins, cellulose, chitin, silk, collagen, and M13 phage) and synthetic piezoelectric materials (such as polylactic acid) are discussed to reveal the underlying electromechanical coupling mechanism at the molecular level, together with typical approaches to the alignment of orientation and polarization to boost their electromechanical performance. Meanwhile, in vivo and in vitro degradation manners of those piezoelectric materials are summarized and compared. Representative developments of typical electronic prototypes leveraging these materials are also discussed. At last, challenges toward practical applications are pointed out together with potential research opportunities that might be critical in this new materials research area.

Keywords

Piezoelectric biomaterials; Biodegradation; Implantable medical devices; Nanogenerator

1. Introduction

Piezoelectric materials are a group of substances that show electric responses (*e.g.*, the accumulation of charges on the surface) when subject to mechanical stress. The early piezoelectric material—Rochelle salt was first synthesized for medical purposes in the late 17th century.[1, 2] It was the Curie brothers who first discovered the piezoelectric effect as

xudong.wang@wisc.edu.

they demonstrated that the effect is closely associated with crystal structures by directly observing the piezoelectric behaviors from solids like quartz, cane sugar, Rochelle salt *etc.*[3] By looking into the crystallography, 20 crystal classes were found to exhibit the direct piezoelectric effect due to the lack of central symmetry in the unit cell, leading to the emergence of perovskite barium titanate (BTO) and the lead zirconate titanate (PZT) family around the world war II.[4–6] Another milestone in the evolution of piezoelectric materials is the discovery of decent piezoelectric coefficients (20–30 pC/N for d_{33} and 16 pC/N for d_{31}) from synthetic polymers, such as polyvinylidene fluoride (PVDF)[7–9]. Nowadays, new inorganic and organic piezoelectric materials with advanced properties and broader functionalities are continuously being discovered and created. [10–12]

Piezoelectrics are essential in the modern society. Statistics show that their market size is expected to reach 27.24 billion US dollars by 2020 from 20.35 billion in 2015, growing at a high compound annual growth rate of 6.01%.[13] Their applications cover extensive fields from automobiles (e.g., tire monitoring,[14] fuel injector[15]) to architectures (e.g., building & bridge oscillation monitoring[16]), from biomedicals (e.g., ultrasonic imaging,[17] wireless pacemaker,[18] and implantable energy harvester[19]) to daily necessaries (e.g., shoes,[19] speakers,[20] igniters,[21] and transformers[22]), and from advanced instruments (e.g., inkjet printer,[23] atomic force microscope[24]) to militaries (e.g., robotics[25]). On the other hand, the raising awareness of lead leaching from the best-performed PZT family is undermining its application potential.[26, 27] Alternative lead-free piezoceramics (BTO and potassium sodium niobate (KNN) based materials) are facing challenges from recycling of their waste while lacking of flexibility.[28, 29] The degradation of PVDF could generates toxic HF that is detrimental to both environment and humanity.[30, 31] As bioelectronics typically interface human bodies, conventional piezoelectric materials have great concerns of biosafety and biocompatibility. In addition, biodegradability, the capability for biological degradation of organic materials by living organisms down to the base substances, is another greatly desired feature, which can circumvent additional surgical procedures and introduce superb biocompatibility and environmental friendliness.[32–35] Therefore, novel piezoelectric materials with ideal biodegradability are the trend for the new generation of implantable and wearable bioelectronics.

Fortunately, small biomolecules like amino acids possess chiral symmetry group, while hierarchical biomaterials such as protein-based polymers (e.g., silk and collagen) and polysaccharides (e.g., cellulose and chitin) forms low-symmetric helical and fibrous structures, exhibiting intriguing piezoelectric effect. Additionally, fast advances in synthetic polymer chemistry allows the design of artificial piezoelectric materials in green and efficient fashions. Those natural or synthetic materials are feasible to be either decomposed into basic molecules like water and carbon dioxide or reabsorbed at biologically benign or physiological conditions. Although most of these materials typically show lower piezoelectric responses compared to the regular commercial piezo-counterparts, approaches such as adjustment in orientation and polarization direction are expected to boost their electromechanical coupling over several orders of magnitudes, enabling the promises for bioelectronics with unique biodegradable properties.

Therefore, in this review, we provide an overview of the most recent major advancements in biodegradable piezoelectric materials. We first introduce different natural and synthetic piezoelectric materials with attempts to understand the underlying electromechanical coupling mechanism at the molecular level. Then, representative implementations of typical electronic prototypes leveraging these materials with enhanced piezoelectricity will be discussed. At last, challenges toward practical applications are discussed together with potential research directions that could facilitate further development. Different from other previous articles that mostly devoted to the progress of piezoelectric biomaterials[36–38], this review focuses on novel piezoelectric biomaterials sharing the unique characteristic of biodegradability, providing insights into their origin of piezoelectricity, as well as new application opportunities as wearable and implantable bioelectronics.

2. Biological Piezoelectric Materials

Biological materials usually have highly ordered structures with low symmetry and lacking an inversion center. Therefore, linear electromechanical coupling is an inherent property of many biomolecules. Since the discovery of piezoelectric effect in natural materials such as cellulose,[39] chitin,[40] and collagen[41] nearly sixty years ago, more and more biological materials have been witnessed with piezoelectricity.

2.1 Amino Acids/Peptides/ Proteins

Amino acids are organic compounds containing amine ($-NH_2$) and carboxyl ($-COOH$) functional groups, along with a side chain (R group) specific to types. They have good solubility in water. There are 20 kinds of amino acids appearing in genetic code of human body. Lemanov *et al.* did pioneering studies on the piezoelectricity of these 20 amino acids by evaluating the piezoelectric response of crystalline powders under high-frequency (~10 MHz) electric pulses.[42–45] Over 16 amino acids and their compounds were found to be piezoelectric at room temperature. Another amino acid—L-methionine even showed moderate piezoelectricity at T<210 K.[46] They also noticed that γ-glycine and DL-alanine have the best performance that is comparable to or even exceeds quartz crystals. These pioneering works inspired later piezoelectric exploration of amino acids.

Piezoelectricity study—Piezoelectricity of glycine has been studied after Lemanov and only modest performances were reported.[47–49] In a most recent work by Guerin *et al*, they revealed the origin of piezoelectricity in glycine and found remarkably high shear piezo-responses.[50] Density functional theory was used to predict the piezoelectric behavior of different glycine polymorphs. Figure 1a shows the space-filling calotte models (CPK model) of glycine crystallizing in three distinct polymorphs, namely, alpha (α), beta (β) and gamma (γ). As shown in the figure, the antiparallel molecular dipoles in the α phase glycine (space group P2$_1$/c) cancel each other and produce no net polarization. β-glycine (space group P2$_1$) has a net polarization along the longitudinal axis which contribute to the 22 piezoelectric coefficient. Similarly, γ-glycine (space group P3$_1$) exhibits a spontaneous polarization along the vertical axis corresponding to the 33 piezoelectric coefficient. Piezoelectric matrixes were calculated for β- and γ-glycine (Fig. 1b). The largest strain coefficient d_{33} in γ-glycine was found to be 10.4 pm V^{-1}, which is comparable to the highest piezo-response of zinc

oxide (Fig.1b). Intriguingly, the predicted shear piezoelectric coefficient d_{16} in β-glycine has a remarkably high value of 195 pm V^{-1} (Fig. 1c). The prediction was verified experimentally by direct piezoelectricity measurements using a piezometer and an impedance analyzer for both β- and γ- glycine (Figure 1d). γ-glycine exhibited d_{11}, d_{22} and d_{33} coefficient of 1.7, −1.1, and 9.93 pmV^{-1}, respectively, agreeing perfectly with the calculated values. Meanwhile, the measured d_{16} in β-glycine was 178±11 pm V^{-1}, also closely matching the calculated number. This value was within the same magnitude of coefficients from many high-performance perovskite ceramics, such as BTO[5] and KNN[51]. The remarkable shear piezoelectricity was attributed to the super-molecular packing in β-glycine that tunes the density, elasticity, and permittivity of the material. Although this β-glycine with ultrahigh piezoelectric response are very promising in electromechanical devices development, one major challenge is its stability, because β phase is metastable and can spontaneously transform into another two phases even in ambient environment.

DL-alanine is another amino acid that has been confirmed with high piezoelectric performance.[46, 52] It crystallizes in orthorhombic symmetry forming a racemic crystal, which renders DL-alanine a nonzero longitudinal d_{33} coefficient together with two transverse (d_{31} and d_{32}) and two shear coefficients (d_{14} and d_{15}). Thompson *et al.* combined DFT calculation and experiment measurements to investigate the piezoelectric properties of this racemic crystals.[53] Compared to L-alanine where molecules pack in antiparallel, there is a strong net dipole in a unit cell of DL-alanine due to the parallel layer alternating between the L and D isomers (Fig. 2a). The spontaneous polarization suggests a high piezoelectricity. Calculation showed that this racemic crystal has piezoelectric coefficients ranging from −1.09 to 17.75 pm V^{-1} (d_{33} around 10.34 pm V^{-1}). More importantly, thanks to the low permittivity (2–3), the theoretical piezoelectric voltage coefficients (up to 0.8 V N^{-1}) could even exceed the values of most PZT ceramics (Fig. 2b). To validate the theoretical prediction, high density films of DL-alanine single crystal needles were obtained from isopropyl alcohol solvent (Fig. 2c). However, the piezometer measurements revealed the average longitudinal d_{33} was relatively low (~ 4 pC N^{-1}). This might because of the randomness of crystal growth where the d_{31} and d_{32} contributions could dilute the real d_{33} values. 9.1 pC N^{-1} of d_{33} has been quantified by piezoresponse force microscopy (PFM) on a single needle, which is in a good consistence with the predicted one. It is worth noting that a single manual compression on the device based on DL-alanine crystal is able to generate 0.8 V response that is higher than most other amino acids. (Fig. 2d)

Strong linear electromechanical coupling was also found in peptide, a compound consisting of at least two amino acids linked by peptide bond. Diphenylalanine (FF) is a peptide discovered from amyloid-β protein in Alzheimers disease,[54, 55] which demonstrated a perovskites-comparable piezoelectricity. This FF peptide tends to form a self-assembled nanostructure, especially nanotubes (Fig. 3a).[55, 56] Molecular simulation of FF solution shows that backbone interaction due to the electrostatic force instead of π-π stacking of phenyl ring drives the initial aggregation, whereas solvent-mediated forces dominate the later crystal growth forming nanotubes (Fig. 3b).[57–59] Kholkin *et al* found the strong shear piezoelectric activity in peptide nanotubes (PNTs) by using PFM to measure the out-of-plane (OOP) and in-plane (IP) polarizations of single nanotubes (Fig. 3c).[60] PNTs with hexagonal crystal symmetry ($P6_1$) showed a strong shear piezoelectricity (d_{15}) along the

tube axis. Nevertheless, the OOP signals representing the longitudinal coefficient was relatively weak. The shear piezo-component was quantified by comparing the response with standard $LiNbO_3$ (LNO) piezoelectric material, because their shear piezo-responses have almost the same dependence on scanning angle α (Fig. 3d). It was found that the shear response of PNT had a strong correlation with the diameter, and the 200 nm PNT exhibited the same d_{15} as bulk LNO (60 ± 10 pm V^{-1}). In addition to hexagonal symmetry, Safaryan *et al.* made use of inkjet printing technology with ethylene glycol as solvent and obtained FF microribbons in another orthorhombic structure.[61] They confirmed that the d_{15} coefficients of orthorhombic FF was around 40 ± 5 pm V^{-1} by PFM measurement, which was also higher than typical PVDF polymers. To quantify the longitudinal response, Semen *et al* placed the PFM tip on the top of a vertical hexagonal PNT and applied an ac voltage sweeping from 0 to 5 V. The d_{33} of 18 ± 5 pm V^{-1} was determined as a slope of the displacement versus voltage amplitude.[62] Several other research also validated that the d_{33} piezoelectric coefficients of FF nanostructures were within the range of 9.9 – 17.9 pm V^{-1}.[63–65]

Proteins are large biomolecules yet still consist of amino acids. Weak piezoelectricity has been observed in lysozyme,[66–68] an antibacterial enzyme widely found in the egg whites of birds and in mammalian tears, saliva and milk. Stapleton *et al* synthesized the lysozyme crystal film with two different crystal structures (tetragonal and monoclinic) following the crystallization protocol outlined by Hampton Research.[66] Piezometer measurements showed that both tetragonal and monoclinic films exhibited weak piezo-responses with an average piezoelectric coefficient of 3.16 pm V^{-1} for the tetragonal phase, while only 0.94 pm V^{-1} for the monoclinic one. The low macroscopic piezo-response of aggregated films could be attributed to the polarization cancellation in different domains and antiparallel arrangement of dipoles in the amino acid basis.

Degradation behavior—One intriguing merit of the piezoelectric amino acid, peptide and protein crystal materials is their descent piezoelectric coefficients together with a relatively low dielectric constant, which could offer extraordinary voltage constants even orders of magnitude larger than the best piezoelectric ceramics available today. Another advantage of these materials is the simple processing approaches that mostly only involve water as the solvent. The Amino acids, peptides and proteins could also gradually decompose into basic molecules in aqueous environment (or biofluids). The residues could either stay with the host system without triggering intense immunogenic responses or be reabsorbed as nutrients. For instance, glycine is a basic nutrient that plays a significant role in neurological function, metabolic regulation, and anti-oxidative reactions. Studies found that glycine is synthesized in many mammals from common biomolecules like serine, choline, and threonine. Glycine is easily catabolized and absorbed mostly through the small intestine where the enzyme glycine cleavage system initiates its degradation to form ammonia and CO_2.[69] Analogously, alanine participated in the essential glucose-alanine cycle between tissue and liver in mammals. Escherichia coli (E. coli), a type of bacteria that normally lives in intestines, can degrade alanine. The catabolism process involves transport, racemization to D-alanine (if the amino acid is L-alanine), and oxidative deamination by D-amino acid dehydrogenase to pyruvate and ammonia, which eventually be utilized as carbon

or nitrogen sources.[70] Therefore, these *in vivo* degradable amino acids/peptides/proteins have great promise being used as components for transient implantable sensors and energy harvesters. However, the instability of those crystals under relatively harsh environment (e.g. piezoelectricity dropping over 70 °C[62, 71] and irreversible phase transition at 140–150 °C [71, 72]) as well as their extremely high rigidity (Young's modulus up to 20 GPa[73]) may raise concerns for their further applications where strategies may need to modify and tuning the downsides.

2.2 Polysaccharides

Polysaccharides are large biomolecules consisting of a large amount of monosaccharide units bonded together by glycosidic linkages. They are the most abundant carbohydrate materials that widely exist in animals, plants, and microorganisms. They have been employed for transient medical applications (*e.g.*, drug,[74, 75] gene,[76, 77] and macromolecule delivery [78], tissue engineering, [79] *etc.*) because of their intrinsic enzymatic degradability. Natural polysaccharides materials like cellulose and chitin have low-symmetry hierarchical fibrous structure exhibiting appreciable piezoelectricity.

Piezoelectricity study—Cellulose has beta glucose as the monomer linked through 1,4 glycosidic bonds and is inclined to form fibril bundles in the wood cell.[80, 81] It is also one of the earliest natural materials found with piezoelectric response.[39, 82, 83] Fukada first quantified the piezo-coefficients in the natural wood as he assumed that the cellulose crystallites in wood oriented with same probability over positive and negative direction along the z-axis while randomly distributed in the x-y plane.[82] This assumption led to non-zero d_{14} and d_{25} (d_{25} = -d_{14}) in the wood matrix and the value was only one twentieth of that of standard quartz. This result was reasonable considering the low cellulose crystallinity and large interferences from other components in wood. The advance in wood technologies enabled the fully extraction of cellulose from wood allowing more precise measurement of its piezoelectricity. Extracted cellulose from wood was found to have two polymorphs, I_α and I_β.[80] I_β has a monoclinic crystal structure. I_α has a non-symmetric triclinic crystal structure yet is a metastable phase that could transform into I_β. Garcia *et al.* predicted the in-layer piezoelectricity of I_β cellulose from a combination of ab-initio and ad-hoc models, and suggested that the piezoelectricity is originated from hydrogen bonding.[84] Their model is presented in Fig. 4a, where the cellulose crystal layers are held by Van der Waals (VdW) interaction, and the in-plane intramolecular interaction is through aligned hydrogen bonding (HB) and inner chain connection is through covalent bonding (CB). The deformation of each single HB under varying electric field in the unit cell was calculated and remarkably high piezoelectricity was discovered ranging from 4.3 to 36.4 pm V^{-1}. Nevertheless, the piezoelectric coefficient of the entire quasi-2D slab was largely influenced by the mechanical constriction inherent to CB along the chain direction. Although relatively low d_{22} (1.3 pm V^{-1}) and d_{11} (0.9 pm V^{-1}) were obtained, they were still comparable to quartz.

On the contrary to low piezo-response from cellulose with amorphous components, a record-high shear piezoelectric constant d_{25} was reported by Csoka *et al* in ultrathin aligned cellulose nanocrystals (CNC) thin films formed with the aids of shear force and electrical field.[85] The piezoelectric response from the CNC film was monitored by measuring the

height deflection using a conductive AFM tip (Fig. 4c). CNC films with an 88% degree of alignment under 800 V/cm at 2 kHz yielded the highest piezoelectric response of 210 pC N^{-1} (Fig. 4d). Although this significantly higher value seems to be inconsistent with previous calculation results, it might be reasonable considering that the measured coefficient was from shear component (d_{25}) while calculated ones were longitudinal coefficients (d_{11} and d_{22}). Nevertheless, this response was only detected at the microscopic scale by AFM. The electrostatic interaction at the AFM tip may have profound interference with the intrinsic piezoelectricity. In addition, moderate piezoelectricity (d_{31}) was also observed in regenerative cellulose with II phase drawn at different ratio by Jaehwan Kim *et al.*[86–89] They investigated the stress-charge behaviors of mechanically elongated cellulose film (electroactive paper) and obtained piezoelectric coefficients from 0.41 pC/N to 7.3 pC/N, corresponding to a drawing ratio from 1.0 to 2.0. (Fig. 4e). However, piezoelectricity enabled by mechanical stretching such as drawing is still controversial, as if there is no favored orientation in the cellulose film, drawing probably only increase the anti-parallel packing of dipoles which together cancel out the net dipole and piezoelectricity.[90]

Like cellulose, chitin is the second most abundant natural polysaccharide that has been produced at 100 billion tons/year. Chitin is composed of N-acetyl-D-glucosamine units through covalent β -(1 → 4)-linkages.[91, 92] It is the building block that strengthens the exoskeletons of crustaceans (shrimp and crab), insects, and the cell walls of fungi (Fig. 5a). [92] Since it shares an analogous structure as cellulose, chitin was also found piezoelectric. There are three polymorphs in the polysaccharides, i.e., α, β, γ. Early in 1970s, Fukada *et al.* reported a weak shear piezoelectricity (less than 0.1 pC N^{-1}) in α-chitin, when they applied an oscillating stress at a frequency of 10 Hz to a chitin sample.[40] A recent DFT calculations by Kim *et al* compared the piezoelectricity in both α- and β-phases of chitin.[93] As presented in Fig. 5b, the net polarization of the ß-conformation in the chitin crystal is strongly uniaxial with a theoretical overall polarization of 1.87 C m^{-2} along the [001] direction. However, the net polar response of α-chitin was weak along all directions of the electric field, which indicated marginal piezoelectricity in α-chitin. Moreover, Kim *et al* used PFM to measure the synthesized β-rich chitin film and revealed a piezoelectric constant of ~4 pm V^{-1} in concert with the calculation.

Degradation behavior—Despite that cellulose is a simple polymer, the numerous intra-/inter-molecular hydrogen bonds inside/between polymer chains render the crystalline microfibrils highly resistant to hydrolysis. While fully biocompatible, cellulose is only degradable by microbial and fungal enzymes.[94] Owing to the lack of hydrolytic enzymes that attack the linkages, the *in vivo* degradation of cellulose in body is rather challenging.[95] Even for organisms having the capability of efficiently degrading cellulose, they have to produce a battery of enzymes with different specificities that work together to enable the degradation.[94] The complete degradation of cellulose into carbon dioxide and water requires synergistic interaction between mixed populations of cellulolytic and non-cellulolytic microorganisms. Although there are studies reporting the *in vivo* degradation of chemically modified cellulose,[96–98] for instance, the oxidized regenerated cellulose formed from nitrogen dioxide treated plant material are feasible to be absorbable and completely degraded over several weeks depending on location and quantity. The inherent

piezoelectricity might be compromised during the specific chemical treatment as both structure, crystallinity and dipoles are altered.

Unlike cellulose, chitin is susceptible to hydrolysis through lysozyme, which is an enzyme ubiquitously existing in mammals. Thus, chitin-based materials are feasible for decomposition *in vivo*.[99–101] Tomihata *et al* did pioneering studies on both in-vitro and in-vivo degradation behavior of chitin and its deacetylated derivatives.[99] They prepared films with a thickness of 150 μm from specimens with different degree of deacetylation (from 0% to 100%). Both experiments were conducted in PBS solution containing lysozyme (in-vitro) and in subdermal tissue of Wistar rats back (in-vivo). It was found that pure chitin exhibited fast decomposition compared to deacetylated derivatives, which had approximately 20% and 50% weight remaining after 30-hour immersing in PBS solution and 2-week implantation in rats, respectively. However, one should note that while the pure chitin has the fast degradation rate, it also triggered the strongest inflammatory tissue reaction at the initial stage around 1 week as rapidly biodegradable biomaterials elicit an acute inflammation reaction due to a significantly large production of low-molecular-weight compounds. This tissue response would decrease after 2 weeks and become very mild after 4 weeks, indicating a relatively good biocompatibility.

Overall, abundance and high biocompatibility are the main merits of piezoelectric polyssacharides. Although there were sporadic reports regarding the high piezoelectricity, effective methods are required to improve their moderate piezoelectric coefficients in order to enable practical applications for bioelectronics.

2.3 Animal-derived polymers

A wide range of animal fibers are made of protein polymers. Unlike the above-mentioned protein crystals, most polymers from animals are semi-crystalline with highly-ordered crystalline regions separated by amorphous amino acid sequences. The piezo-active organic polymer matrix, collagen, is a typical example of such polymers, which is responsible for the piezoelectric effect found in bones over fifty years ago.[41, 102, 103] Other animal-derived polymers with a similar structure as collagen, have also been discovered piezoelectric. Here, silk and collagen, the two most-studied and widely-used animal polymers, and the origin of their piezoelectricity will be discussed.

Piezoelectricity study—As a material closely associated with human history, silk had a long history of application that could date back to 8500 years ago in China. The structure of silk, fully unveiled until the recent two centuries, was demonstrated to have three configurations, namely, the water-soluble silk I, the crystalline silk II, and the amphiphilic silk (Fig. 6a).[104, 105] The mechanically unstable silk I only contains random-coil of protein polymers forming an amorphous structure. Silk III with threefold helical chain conformation usually act as surfactant at the air-water interface during silk processing. Only the silk II structure contains high-crystalline antiparallel β-sheet arranging in a monoclinic unit cell. Fukada *et al* conducted the first measurement of the piezoelectricity from orientated silk bundles.[106] Their silk fibers were dried for weeks in a desiccator containing calcium chloride, and polarization was observed when pressure was applied on the bundles in a

direction 45 degree away from the orientation axis of fibers. Although they obtained a fair shear value of piezoelectricity of ~1 pC N^{-1}, the correlation between the piezoelectric response and active silk components was not scrutinized.

In a recent study by Yucel *et al*, the structural origin of silk piezoelectricity was revealed.[107] They developed a zone-drawing device that enabled drawing of silk films to a desired ratio at high temperatures. Fourier-transform infrared spectroscopy (FTIR) and wide-angle X-ray diffraction (WAXD) together confirmed the strong positive correlation between silk II β-sheet content and the draw ratio λ. The film drawn to the highest ratio of 2.7 before broke exhibited the largest shear piezoelectricity d_{14} of ~−1.5 pC N^{-1}, corresponding to an increase in d_{14} of over two orders of magnitude (Fig. 6a) from original films. The FTIR and WAXD results showed the increase of II β-phase crystallinity at higher drawing ratio. This work showed that mechanical drawing is an effective approach to induce piezoelectricity in silk fibers, and the silk piezoelectricity is closely related to the combination of high β-sheet crystal content and crystal orientation (Fig. 6b). In analogy to previously discussed drawn cellulose film, if there is no favored orientation in the silk film, drawing is only able to increase the anti-parallel packing of dipoles, leading to reduced net dipole. At the meanwhile, one should also note that a relatively low measurement frequency was employed at their work (0.5 Hz) compared to typical piezoelectric tests (above 30 kHz[108, 109]). As other electromechanical couplings such as ion migrations, electrostatic effect and interfacial polarization are sensitive to low frequency stimuli, they may interfere with intrinsic piezoelectricity and lead to inaccurate test result. Thus, the reported shear piezoelectricity of silk here might not be intrinsic. In addition, repolarization of silk fibers under a high electrical field was reported by Pan *et al*.[110] A superior arrangement of β-sheet in the silk fiber poled by a 3×10^6 V/m electrical field led to three times higher electrical potential (40.7 mV) compared to the one without poling (13.4 mV).

Collagen as another protein-based polymer, commonly exists in organs/tissues of mammals such as bone, skin, and cartilage. In an early study by Marino and Becker, the piezoelectric response of human bones was tested after either demineralization or decollagenation.[103] They found that the piezoelectricity in bones might completely arose from the organic component—collagen. Even inorganic hydroxyapatite nanocrystals in bones was observed with piezoelectricity later[111–113], collagen was still believed to play a major role in the electromechanical coupling of bones. In 2002, Kumar *et al* used molecular dynamics (MD) to understand the piezoelectric behavior of collagen.[114] They found that the piezoelectric effect in short collagen fibrils was determined by reorientation of the backbone polar groups in response to mechanical stress. Nevertheless, their simulation model (a short chain simply incorporating a sequence of three types of amino acids) was rather ideal and basic to represent the real scenario. Zhou *et al* later built a more complicated, right-handed, super-twisted collagens model to unveil the native collagen piezoelectricity at the molecular level (Fig. 7a).[115] The simulation revealed that collagen fibril has spontaneous uniaxial polarization along the long axis. They also pointed out that the mechanical stress-induced reorientation of the permanent dipoles inside individual polar residues gave rise to the longitudinal piezoelectric coefficient d_{33} of ~2.64 pC N^{-1} (Fig. 7b).

A total of 28 types of collagen[116, 117] with high hierarchy have been discovered displaying various mechanical properties, allowing for diverse piezoelectric activities. For instance, Denning *et al* discovered decent piezoelectricity from rat tail tendons (majority of type I collagen).[118] By sectioning rat tail tendons at angles of 0, 59, and 90 degree relative to the plane orthogonal to the major axis, piezoelectricity was measured from those samples by PFM (Fig. 7c). Two different domains representing opposite polarizations were clearly observed by PFM. Both in-plane and out-of-plane piezoresponse as a function of applied AC voltage was measured, from which the piezoelectric coefficients d_{33} and d_{31} were estimated to be 0.89 ± 0.08 pC N^{-1} and -4.84 ± 2.96 pC N^{-1}, respectively (Fig. 7c). The macroscopic piezoelectric response of scleral tissue (types I, III, V, and VI collagen incorporate[119]) from human and bovine eyes investigated by Ghosh *et al* presented an order of magnitude higher value with a d_{31} up to 31.8 pC N^{-1}.[120] While both human and bovine samples had decent piezoelectric coefficients that were comparable to PVDF, the response decreased as a function of time when the sample became dehydrated. Denning *et al* further compared the piezoelectricity of individual type I and type II (mostly in cartilage) collagen fibril by harnessing the PFM.[121] 3D topography images overlaid with d_{15} piezoelectric coefficient maps showed that type I collagen had significant higher shear piezoelectricity than type I collagen. Specifically, the lateral PFM measuring the amplitude as a function applied AC voltage revealed that the average shear coefficient for type I (2.2 ± 0.5 a.u.) was approximately 68% higher than that of type II (0.7 ± 0.2 a.u.). It was attributed to the different polypeptide chains with less dipole and more covalent crosslinks that impeded mechanical deformability and lowered piezoresponse in type II collagen.

Degradation behavior—Both silk and collagen belong to enzymatically degradable polymers that require catalysis to undergo effective degradation under physiological conditions. For instance, silk is susceptible to proteolytic enzymes such as chymotrypsin, actinase, and carboxylase.[122–124] In vitro studies revealed that the amorphous region of silk could be digested quickly in the first few days in an enzyme solution[125], while the highly ordered crystalline region requires longer time (over 15 days) for digestion[126]. Specifically, Minoura *et al* prepared silk fibroin membrane through casting from the diluted liquid silk solution and dried at 25°C. Exposed to a neutral Pronase E solution at 37 °C, they compared the *in-vitro* degradation behaviors of as-prepared silk fibroin membrane with commercial silk suture. It was found that the weight of silk fibroin membrane sharply decreased over the first few days followed by leveling off at 90 percent of original value. They attributed the fast weight loss to the quick digestion of molecules in the amorphous region, while remained weight belongs to crystalline area. This was evidenced by the degradation behavior of high crystallized silk suture as almost no digestion or surface morphology change was observed. Compared to *in vitro* degradation through enzymatic solution, *in vivo* degradation of silk is usually induced by the foreign body reaction mechanism, the degradation process would not lead to significant immunogenic response. The final degradation products are amino acids which are easily absorbed by the host. However, the *in vivo* decomposition of silk materials always requires a long period of time from several months to years. Wang *et al* studied the degradation of silk scaffold in nude mice and Lewis rats, and they found distinctive degradation behaviors of silk fabricated from different processes.[127] While most silk scaffolds prepared from an all-aqueous process completely disappeared between 2 to 6

months, those processed in organic solvent (hexafluoroisopropanol (HFIP)) could last beyond 1 year. Those results indicated the effective tuning of biodegradation behavior among silks through adjusting their crystallinity and processing methods.

Compared to silk-based materials, *in vivo* degradation of collagen (collagenolysis) has a relatively rapid rate. Through studying radiolabeled proline as a key component in collagen, the skin collagen degradation rate (metabolism rate) in adult rats was found typically between 3 and 5% per day.[128] Nevertheless, the degradation behavior of foreign implants consisting of collagen is different. Alberti *et al.* studied the biodegradation of scaffolds comprised of highly aligned collagen fibrils in Sprague–Dawley rats.[129] The scaffolds were made of decellularized tendon using a slicing, stacking and rolling technique. They found that the crosslinking of collagen by glutaraldehyde could largely improve the stability. While the non-crosslinked collagen scaffolds rapidly degraded and lost the fiber morphology in three weeks; the crosslinked samples remained intact for nine weeks.

Despite that the piezoelectric coefficients of silks and collagens were generally lower compared to commercial piezoelectrics, their excellent biocompatibility, controllable biodegradability, and almost zero immunogenic degradation byproducts still make animal-derived polymer a promising candidate for bioelectronics. Moreover, the diversity in collagen also provides more building blocks for designing functional devices with desired mechanical and piezoelectric properties.

2.4   Virus

Virus has the simplest structure of living beings with a nucleic acid genome as the core and an outside protein protection layer (capsid). Nowadays, virus has found great values in biomedicals. For instance, viruses could be engineered as an effective vehicle to deliver a specific gene to infected cells offering new possibilities of treating diseases.[130–132] The capsid consisting of highly-ordered proteins endowed piezoelectric response in certain viruses and enabled their great potential in functional bioelectronics.

Piezoelectricity study—M13 bacteriophage is a virus that exhibits strong piezoelectricity.[133–135] The protein coating of M13 could be functionalized with a broad range of molecules in a very mild biocompatible environment, and thus expand the application of M13 phage in medicals and synthetic biology.[136] Its piezoelectricity was studied by Lee *et al* first in 2012.[133] The protein pVIII coated on M13 phage has an α-helical structure with a net dipole moment from amino-end (negative) pointing to the carboxyl-terminal (positive) (Fig. 8a). PFM characterization on phage virus displayed strong piezoelectric response at both lateral and axial directions indicating the existence of longitudinal and shear piezoelectricity. Since the bacteriophage has a good engineerability, two additional negatively charged amino-acid glutamate (E) could be added to its amino-terminals forming a 4E-phage with enhanced polarization. While a monolayer of unmodified phage has an effective piezoelectric coefficient (d_{eff}) around 0.30 ± 0.03 pm V^{-1}, the 4E-phage exhibited more than 2-times larger value of 0.70 ± 0.05 pm V^{-1}. Additionally, the piezoelectric property could be further improved by increasing the thickness of the phage film. When the thickness reached 100 nm, the coefficient of a wild type phage film surged

up to a saturated level of $d_{33} \approx 7.8$ pm V^{-1} (Fig. 8c). Likewise, the 4E phage film with similar pattern exhibited an extraordinarily high d_{33} value of 13.2 pm V^{-1} that was 10 times higher than the collagen film with the same thickness (1.1 pm V^{-1}) (Fig. 8d). This high-performance phage film also demonstrated reverse piezoelectric effects. This multifunctionality and good tunability opens many possibilities for integration into bioelectronic devices as energy harvester, actuator, and transducer.

Degradation behavior—Since M13 phages are viruses only infect bacteria without attacking eukaryotic cells, they are widely exploited for diagnosing and therapeuticizing. The biodegradability of M13 phage in different body fluids and tissues was systematic studied by Celec *et al. in vitro*,[137] as the first study in this field where very few reports have existed. They analyzed the survival of M13 phage in different body fluids and tissues *in vitro*, including blood, saliva, urine, and homogenates of stomach, jejunum, and colon. Whereas there was almost no decrease in the sterile phosphate-buffered saline (PBS) control group, the experiment groups exhibited obvious degradation to various degree. While the M13 phage decreased 44%, 66% and 88% after 45 min in blood, urine and saliva, respectively, the most rapid phage degradability was observed in jejunum homogenate with nearly one hundred percent degradation after 45 min, attributing to the abundant proteolytic enzymes in the homogenate. This rapid degradation suggests the feasibility of bacteriophages for constructing *in vivo* transient therapeutic devices.

Although virus has exciting piezoelectric responses, it should be noted that piezoelectricity of phage film was not fully understood at the molecular level currently. The ordered phage with D_6 or C_6 symmetry still could not completely explain the piezoelectric behaviors observed experimentally. In-depth mechanism studies are required to completely unveil the phage piezoelectricity to lay the foundation for their future applications.

3. Synthetic Biodegradable Piezoelectric Polymers

Beyond nature biomaterials, most polymers are designed and synthesized in laboratory, which offers great versatility in tailoring the materials' properties. Similarly, synthetic polymers with intrinsic dipoles could exhibit piezoelectricity by adjusting the configuration/conformation of polymer chains. Mimicking how biological piezoelectric materials produce polarizations upon straining, desired biodegradability could be introduced to synthetic piezoelectric materials.

While lactic acid is a common human metabolic byproduct, its polymerization could lead to the formation of semi-crystalline polymers - polylactic acid (PLA).[138, 139] Bonded together by ester bonds in the main polymer chain, the PLA would undergo hydrolytic degradation (a bulk erosion mechanism by random scission of backbone) when subjects to microbial attacks or reacts with water.[34, 140] It could eventually be broken down to basic molecules such as water and carbon dioxide. Because lactic acid is a chiral molecule with two enantiomers: the naturally occurring L-lactic acid and synthetic D-lactic acid, condensation of isomers with the same conformation could yield two conformations, *i.e.*, poly(L-lactic acid) (PLLA) and poly (D-lactic acid) (PDLA). Strong shear piezoelectricity could be

expected from the aligned electrical dipoles in the carbon–oxygen double-bonds (C = O) branching off from the polymer backbone (Fig. 9a). [141–144]

Piezoelectricity study

Experimental measurements revealed that the 0-cut PLLA specimen with a side along the z-axis (elongation direction) had an appreciable shear piezoelectric coefficient d_{14} of 9.82 pC N^{-1}.[145] Curry *et al* recently investigated the impact of drawing ratio (elongation ratio, λ) on its piezoelectricity.[146] As illustrated in Fig. 9b, the raw PLLA film exhibited three crystal faces (111), (200), and (110). As the drawing ratio increased, the intensity of the (111) peak declined significantly, indicating the transformation from α-phase incorporating a left-handed 10_3 helical conformation to β-phase with a 3_1 helical conformation. Meanwhile, the crystallinity of PLLA film maximized at a drawing ratio of 5 and then decreased with further elongation. Shear stress was applied to films with different drawing ratios and the generated electric potentials were monitored (Fig. 9c). The best piezoelectric effect was obtained in the λ range of 2.5–4.5, consistent with crystallinity evolution. The results evidenced that uniaxial deformation could help the alignment of polymer chains with polar C=O bonds and thus enhances the piezoelectricity. Advanced characterization techniques further enabled direct observation of PLLA piezoelectricity at the micro/nano-scale.[147, 148] Smith *et al* reported the measurement of shear piezoelectricity in highly crystalline and orientated PLLA nanowires by PFM.[147] They grew the nanowires in confined anodized aluminium oxide (AAO) template, where the nanoconfinement promoted crystallinity that was proved to be 70%. Under PFM, significant defection was seen in the lateral signal along the nanowire while only sharp vertical response was detected at the edge of nanowire, indicating a strong shear piezoelectricity (Fig. 9e). Deflection gradient under AC voltage sweeping gave an estimated d_{14} around 8 pC N^{-1}, the same as that of bulk materials.

Degradation behavior

As a representative synthetic biodegradable polymer, the PLA family has well-known and long-standing experiences in medicals. The PLLA experienced slow hydrolysis when reacted with water in tissue.[149–151] Bos *et al.* studied *in vivo* long-term degradation of PLLA by subcutaneously implanting high-molecular-weight samples (used for internal fixation of fractures) on the back of rat.[152] An apparent decrease in molecular weight as well as mass was observed at the initial stage (first 3 months), which was attributed to the pure hydrolysis. Resorption was responsible for the continuous mass loss from 26 weeks, whereas no chronic or acute inflammatory reactions were found until 104 weeks when macrophages appeared and participated in cleaning remaining PLLA particles. Like many other biodegradable polymers, the amorphous region disintegration dominated the beginning while the left particles eventually removed by macrophages are highly crystalline. In addition, previous studies also have demonstrated that PLLA implants could last for 5.7 years with good biocompatibility before being fully disintegrated by patients.[153] Analogous to the results of above mentioned rat experiment, the PLLA implants would be eventually converted to a small fraction of highly crystallized particles which are not absorbable but could be cleaned away by immune system.

Overall, the appreciable degradation behavior coupled with unprecedented piezoelectricity is expected to provide more possibilities in implantable bioelectronics, especially for in-vivo therapeutics and electric energy generation among PLLA.

4. Bioelectronic applications

Bioelectronics refer to electronics consisting of biological/bio-inspired organic/inorganic materials that interface with biological system. It could function as sensor/actuator/other information processing system to detect and collect biological signals.[154–156] However, there is a paradigm shift in current bioelectronics from old-fashioned unrecyclable devices to green and sustainable intelligent devices with more functionalities.[157–161] The above-mentioned biodegradable and bioabsorbable piezoelectric materials, a gift endowed by nature and science, are foreseeable to be playing a vital role in the futuristic bioelectronics design and manufacturing.

4.1 Nanogenerators for biomechanical energy harvesting

Owing the linear electromechanical coupling, piezoelectric biomaterials could convert mechanical energy into electricity, and thereby functioning as a nanogenerator. FF peptide has a decent piezoelectric response comparable to other commercial polymeric piezoelectrics such as PVDF[162], and it was considered as a promising biomaterial for mechanical energy harvesting. [60–65] Nguyen *et al* developed an effective approach that enables good alignment of FF and dipoles therein at wafer-scale and fabricated high-performance green power generator based on vertically aligned microrods.[65] They first coated a wafer substrate with an FF seed film and subsequently grew FF microrods on the seed film in a concentrated water solution. During the growth, an electrical field of 2 kV/cm for dipole alignment was applied along the normal of substrate. A uniform FF film exhibiting a high d_{33} of 17.9 pm V^{-1} with vertically aligned microrods (Fig. 10a) was obtained under positive electrical field. A nanogenerator was built by sandwiching the FF film between two gold electrodes (Fig. 10b). When a force of 60 N was applied, the nanogenerator generated an open-circuit voltage (V_{oc}) up to 1.4 V and a short-circuit current (I_{sc}) of 39.2 nA, together contributing a power density of 3.3 nW cm^{-2} (Fig. 10c). The power provided by three stacking under finger typing had the ability to operate a liquid crystal display (LCD), showing the potential capability as a power supply for small electronics. Similarly, an energy harvester was fabricated by Lee *et al* based on large-scale aligned FF nanotubes (Fig. 10e),[163] which was fabricated by a simple method of pulling a substrate vertically out of concentrated solution. The aligned FF nanotubes exhibited unidirectional polarization under PFM scanning, and a strong piezoelectric component (d_{15}) of 46.6 pm V^{-1} was detected (Fig. 10f). The final device was built after the nanotubes were coated with poly(vinylpyrrolidone) (PVP) protection and sandwiched between Au/Cr electrodes on flexible polymer substrates. A higher electrical output (V_{oc} = 2.8 V, I_{sc} = 37.4 nA and power around 8.2 nW) under a small stimulus (Force = 42 N) was obtained from a single device, which was sufficient to power an LCD panel.

In addition to FF peptide, virus has also been demonstrated as a promising building block for mechanical energy harvesting due to their good capability for chemical modification, which

may enable a large range of tunable dipole moment. Shin *et al* developed a piezoelectric nanogenerator (PNG) based on vertically aligned M13 bacteriophage nanopillars. An AAO porous nanostructure was used as a template to deposit the 4E-phages on the fluted channels to form dense virus nanopillars.[135] Controlling the infiltration cycles as well as the virus solution concentration, the average height of the nanopillars was adjusted from ~2 to ~50 μm (Fig. 11a). A robust PNG device was made after depositing electrodes on porous template and being encapsulated by polydimethylsiloxane (PDMS) elastomer. It output an average V_{oc} of 232 mV and I_{sc} of 11.1 nA at an applied force of 30 N. The maximum power output around 0.99 nW was record at a load resistance of 10 MΩ. This level of power output might be useful for miniaturized sensor nodes but it was still relatively low compared to peptide based devices. Lee *et al* recently improved the output of virus-based power generator by several orders of magnitude by realizing a better dipole arrangement.[134] The improvement of dipole arrangement was attributed to the monolayer assembly of vertically aligned M13 phages that was driven by upward capillary force during the evaporation of solution under a micropatterned PDMS. PFM results showed that the assembled 6H-phage had a d_{eff} of 13.2 pm V^{-1}, significantly outperformed the wide type random phage films (0.35 pm V^{-1}). Before device fabrication, the unidirectionally orientated phages were crosslinked by dityrosine to enhance the mechanical property. The PNG was fabricated by inserting the aligned 6H-phage/PDMS film in between Au/Cr coated polymer substrates (Fig. 11f). Extraordinarily high electrical output was generated, with the voltage, current and power reached 2.8 V, 120 nA and 236 nW (Fig. 11g), respectively. Five devices connected in series could charge a 100 μF capacitor to 5V within 8000 s (Fig. 11h). They were able to power a commercial light-emitting diode (LED) and drive an LCD panel to operate, showing the capacity as a power supply equivalent to small batteries.

In summary, PNG prototypes leveraging biodegradable piezo-materials could generate electricity at the nanowatts level. This power output might be smaller than other energy harvesters such as electromagnetic[164–166] and triboelectric generators.[167–170] However, the unique possibility of integrating these piezoelectric materials with common biodegradable encapsulation materials (such as PLA, PCL, PLGA *et al*) and biodegradable electrodes (such as iron, magnesium, conducting polymers *et al*) is capable of creating novel biodegradable devices with desired performance, providing new opportunities in battery-free self-powered transient implantable bioelectronics.[159]

4.2 Actuator, sensor and transducer

Biodegradable piezoelectric materials have also been applied in the development of actuator, transducer and sensors for biomedical applications. Tajitsu *et al* developed a smart medical tweezer/catheter based on PLLA fibers.[171–173] Using high-speed spinning, they obtained PLLA fibers with improved piezoelectricity. Two rectangular electrodes were deposited on the upper surface of a single PLLA fiber with a diameter of 40 μm to make an actuator. They observed apparent vibration from the PLLA fiber when an AC voltage in the range of 50 – 300 V was applied at a frequency of 0.1 – 150 Hz. Based on this design, a PLLA actuator was fabricated to function as a medical tweezer which was able to gasp and remove thrombosis sample under microscope (Fig. 12a). The micro PLLA actuator demonstrated a great potential as smart implantable transient devices for cleaning the blocked blood vessels.

The *in vivo* degradation behavior of the PLLA fibers was demonstrated by Ishi *et al* who subcutaneously implanted the fibers in Wistar rats for 12 weeks.[174] The tissues stained by Hematoxylin and eosin (HE) showed that delamination occurred on the surface of the PLLA nanofiber after 4-week implantation and severe damages of structure with tissue infiltration was observed on 12-week implantation owing to the degradation (Fig. 12b). The complete dissociation of fiber structures and the significant decrease of fiber crystallinity and molecular weight confirmed the *in vivo* biodegradation.

The application of PLLA as a biodegradable implantable force/pressure sensor was also demonstrated by Curry *et al*.[146] They affixed molybdenum pieces on a piezoelectric PLLA film as electrodes and encapsulated the PLLA/Mo assembly by PLA to enable implantation (Fig. 12c). The *in vivo* pressure sensibility was illustrated by inserting the packaged device into an incision below the mouse's diaphragm. A clear signal was detected when the mouse breath under anesthesia, which was correlated to a sinusoidal force of ~0.1 N cm^{-2} (Fig. 12d). In addition, the PLLA film was fully degraded in 56 days in the phosphate-buffered saline (PBS) at a temperature of 74 °C. The implantability was evidenced by a mild immune reaction without significant presence of inflammation during the 2–4 weeks implantation in mice.

Kim *et al* applied biocompatible electroactive chitin film for audio transducers.[93] The β-rich chitin film (4×6 cm^2) was obtained from squids, with which a transparent transducer was fabricated using silver nanowires as electrodes (Fig. 12e). The short-time Fourier transformation (STFT) revealed that the sound waves generated by the chitin device well matched the original sound source with 71% synchronization, indicating its potentials for speaker applications (Fig. 12f). In addition, the electroactive chitin film would fully disintegrate in a water solution containing a small amount of chitinase enzyme within eight days at room temperature, evidencing the potential for naturally degradable bioelectronics. Apparently, this flexible chitin film could be further exploited as building blocks for self-powered wearable technology for biological signal (such as voice and motions) detecting and analyzing.

More implementations of these advanced biodegradable piezoelectric materials as intelligent monitor[143, 144], smart wearable antibacterial textile[142], and even devices in tissue engineering[156] are now becoming popular strategy to enabling biocompatibility and degradability while remain a desired performance.

5. Conclusion and Perspectives

Although the exploration starts as early as in 1950s, the underlying mechanism of piezoresponse in biodegradable materials was not clear during the past half century. Deep understanding of piezoelectricity in soft materials nowadays allowed better engineering of these materials to meet specific electronic applications. Many exciting demonstrations of their versatile abilities such as high-efficiency energy harvesting, controllable actuation and high mechanical-stimulus sensitivity opened intriguing applications for introducing biodegradation ability to biomedical devices that were usually built upon hard ceramic

piezoelectrics. Despite these intriguing potentials, both the natural materials and the synthetic biopolymer are still facing major challenges and problems below:

1. Current piezoelectric biomaterials are still much more rigid compared to human tissues and organs. For instance, the self-assembled peptide has a Young's modulus of ~19 GPa[73] and the Modulus in synthetic PLLA is also in the GPa level[175, 176]. The Young's modulus of some hydrated collagens could be at a lower level of 20–200 MPa,[177, 178] however, it is still 1–2 orders of magnitude higher than soft skin and brain. Besides, desired high piezoelectric performance is always in conflict with flexibility and softness, as high piezoelectricity corresponds to high crystallinity while flexibility and softness favors amorphousness in semi-crystalline polymers. How to enable the biomimetic property while keep the high piezoelectricity is of great importance for future self-powered implantable medical devices (IMDs) and wearable electronics.

2. Most natural and synthetic organic piezoelectric materials have strong shear components yet weak transverse and longitudinal responses. Take the glycine as an example, the shear piezoelectricity in β polymorph (178 pC N^{-1}) is 2 orders of magnitude higher than the longitudinal one (4.7 pC N^{-1}). Some orientated materials even only show shear piezoelectricity. Nevertheless, considering that the normal out-of-plane stress is the most common mechanical stimuli, specific device configurations are required to translate the normal stress into in-plane shear in piezoelectric device design, which might either lower the efficiency or complicate the device fabrication.

3. Stability and durability are of great concern for the biodegradable piezoelectric materials. Many of their polymorphs with strong piezoelectricity are metastable. For example, β-glycine can gradually transform to γ or α phase even at room temperature. In addition, many practical applications of electromechanical coupling devices require a large number of strain cycle lifetime, which may deteriorate the piezoelectric performance of peptide materials that has a relatively low stability. Moreover, most biomaterials could not survive in relatively harsh environment such as high temperature. This also happens to the synthetic PLLA that only has a low glass transition temperature at ~60°C.[179, 180] Typically, a robust encapsulation with matching mechanical properties needs to be developed to improve the durability and stability.

4. More effective approaches are required to manage the dipole/polarization in the biomaterials to enable higher piezoelectric performance. Despite that external mechanical forces such as shear force and capillary force could facilitate molecular orientation, these mechanical stimuli have weak interactions with polarization. As a result, polar groups may exhibit an antiparallel conformation, canceling out the effective dipoles for macroscopic piezoelectricity generation. Methods reasonably incorporating both mechanical and electrical forces could be a good solution to achieve a good control over both orientation and dipole moment and eventually lead to optimal performance.

5. More robust protocols for piezoelectric response measurement of biomaterials should be established to rule out interferences from other factors. The reported piezoelectric coefficients for the same materials could vary over several orders of magnitude[90], such as cellulose and collagen. Due to the rich number of polymorphs in these materials and different measurement approaches at various length scales (macroscopic (PFM)/microscopic (piezometer)), other electromechanical coupling effects might impose large impacts to the results. Intrinsic (e.g. electrostriction and flexoelectricity) and extrinsic contributions (e.g. electrochemical ion migration and electrostatic effects) should be avoided in order to establish a reliable relationship between materials and their piezoelectric properties.

While challenges still exit, employing advanced technologies such as high performance computing (HPC) and additive manufacturing (3D printing) [181–183] to design and fabricate piezoelectric materials with programmable lifetime and enhanced piezoelectric behavior could open more opportunities for biodegradable and bioabsorbable bioelectronics. These type of functional materials and devices will play a vital role in futuristic bioelectronics for health monitoring, therapeutic and cosmetic applications.

Acknowledgement:

References

1. Busch G, Early history of ferroelectricity. Ferroelectrics 1987, 74, 267–284.

2. Valasek J, Piezo-electric and allied phenomena in Rochelle salt. Physical review 1921, 17, 475.

3. Mason WP, Piezoelectricity, its history and applications. The Journal of the Acoustical Society of America 1981, 70, 1561–1566.

4. Haertling GH, Ferroelectric ceramics: history and technology. Journal of the American Ceramic Society 1999, 82, 797–818.

5. Acosta M; Novak N; Rojas V; Patel S; Vaish R; Koruza J; Rossetti G Jr; Rödel J, BaTiO3-based piezoelectrics: Fundamentals, current status, and perspectives. Applied Physics Reviews 2017, 4, 041305.

6. Von Hippel A; Breckenridge R; Chesley F; Tisza L, High dielectric constant ceramics. Industrial & Engineering Chemistry 1946, 38, 1097–1109.

7. Kepler R; Anderson R, Piezoelectricity and pyroelectricity in polyvinylidene fluoride. Journal of Applied Physics 1978, 49, 4490–4494.

8. Kepler R; Anderson R, Ferroelectricity in polyvinylidene fluoride. Journal of Applied Physics 1978, 49, 1232–1235.

9. Kawai H, The piezoelectricity of poly (vinylidene fluoride). Japanese journal of applied physics 1969, 8, 975.

10. Liao W-Q; Zhao D; Tang Y-Y; Zhang Y; Li P-F; Shi P-P; Chen X-G; You Y-M; Xiong R-G, A molecular perovskite solid solution with piezoelectricity stronger than lead zirconate titanate. Science 2019, 363, 1206–1210. [PubMed: 30872522]

11. Ye H-Y; Tang Y-Y; Li P-F; Liao W-Q; Gao J-X; Hua X-N; Cai H; Shi P-P; You Y-M; Xiong R-G, Metal-free three-dimensional perovskite ferroelectrics. Science 2018, 361, 151–155. [PubMed: 30002249]

12. Zhang H-Y; Tang Y-Y; Shi P-P; Xiong R-G, Toward the Targeted Design of Molecular Ferroelectrics: Modifying Molecular Symmetries and Homochirality. Accounts of chemical research 2019.

13. McWilliams A, Smart materials and their applications: technologies and global markets. BCC Research Advanced Materials Report 2011, 161.

14. Yang Z; Zhou S; Zu J; Inman D, High-performance piezoelectric energy harvesters and their applications. Joule 2018, 2, 642–697.

15. Senousy M; Li F; Mumford D; Gadala M; Rajapakse R, Thermo-electro-mechanical performance of piezoelectric stack actuators for fuel injector applications. Journal of Intelligent Material Systems and Structures 2009, 20, 387–399.

16. Iqbal M; Khan FU, Hybrid vibration and wind energy harvesting using combined piezoelectric and electromagnetic conversion for bridge health monitoring applications. Energy conversion and management 2018, 172, 611–618.

17. Zhou Q; Lam KH; Zheng H; Qiu W; Shung KK, Piezoelectric single crystal ultrasonic transducers for biomedical applications. Progress in materials science 2014, 66, 87–111. [PubMed: 25386032]

18. Li N; Yi Z; Ma Y; Xie F; Huang Y; Tian Y; Dong X; Liu Y; Shao X; Li Y, Direct Powering a Real Cardiac Pacemaker by Natural Energy of a Heartbeat. ACS nano 2019, 13, 2822–2830. [PubMed: 30784259]

19. Li J; Wang X, Research Update: Materials design of implantable nanogenerators for biomechanical energy harvesting. APL materials 2017, 5, 073801. [PubMed: 29270331]

20. Ko SC; Kim YC; Lee SS; Choi SH; Kim SR, Micromachined piezoelectric membrane acoustic device. Sensors and Actuators A: Physical 2003, 103, 130–134.

21. Tan Y; Hoe K; Panda S In Energy harvesting using piezoelectric igniter for self-powered radio frequency (RF) wireless sensors, 2006 IEEE International Conference on Industrial Technology, IEEE: 2006; pp 1711–1716.

22. Yang J, Piezoelectric transformer structural modeling-A review. IEEE transactions on ultrasonics, ferroelectrics, and frequency control 2007, 54, 1154–1170.

23. Saunders RE; Gough JE; Derby B, Delivery of human fibroblast cells by piezoelectric drop-on-demand inkjet printing. Biomaterials 2008, 29, 193–203. [PubMed: 17936351]

24. Binnig G; Quate CF; Gerber C, Atomic force microscope. Physical review letters 1986, 56, 930. [PubMed: 10033323]

25. Wu Y; Yim JK; Liang J; Shao Z; Qi M; Zhong J; Luo Z; Yan X; Zhang M; Wang X, Insect-scale fast moving and ultrarobust soft robot. Science Robotics 2019, 4, eaax1594.

26. Kosec M; Malic B; Wolny W; James A; Alemany C; Pardo L, Effect of a chemically aggressive environment on the electromechanical behaviour of modified lead titanate ceramics. JOURNAL-KOREAN PHYSICAL SOCIETY 1998, 32, S1163–S1166.

27. Rödel J; Webber KG; Dittmer R; Jo W; Kimura M; Damjanovic D, Transferring lead-free piezoelectric ceramics into application. Journal of the European Ceramic Society 2015, 35, 1659–1681.

28. Okada K; Yanagisawa T; Kameshima Y; Nakajima A, Properties of TiO2 prepared by acid treatment of BaTiO3. Materials Research Bulletin 2007, 42, 1921–1929.

29. KIKUTA K; SHIMIZU Y; MORIYA M; YAMAGUCHI T; HIRANO S-I; SAITO Y; MIYOSHI T; YAMAMOTO H; SAKABE Y, Low temperature recycling process for barium titanate based waste. Journal of the Ceramic Society of Japan 2006, 114, 392–394.

30. Liu F; Hashim NA; Liu Y; Abed MM; Li K, Progress in the production and modification of PVDF membranes. Journal of membrane science 2011, 375, 1–27.

31. Madorsky S, Fluorocarbon and chlorocarbon polymers Thermal degradation of organic polymers, John Wiley & Sons Inc 1964, 130–172.

32. Tan MJ; Owh C; Chee PL; Kyaw AKK; Kai D; Loh XJ, Biodegradable electronics: cornerstone for sustainable electronics and transient applications. Journal of Materials Chemistry C 2016, 4, 5531–5558.

33. Feig VR; Tran H; Bao Z, Biodegradable polymeric materials in degradable electronic devices. ACS central science 2018, 4, 337–348. [PubMed: 29632879]

34. Nair LS; Laurencin CT, Biodegradable polymers as biomaterials. Progress in polymer science 2007, 32, 762–798.

35. Middleton JC; Tipton AJ, Synthetic biodegradable polymers as orthopedic devices. Biomaterials 2000, 21, 2335–2346. [PubMed: 11055281]

36. Ciofani G; Menciassi A, Piezoelectric nanomaterials for biomedical applications. Springer: 2012.

37. Ribeiro C; Sencadas V; Correia DM; Lanceros-Méndez S, Piezoelectric polymers as biomaterials for tissue engineering applications. Colloids and Surfaces B: Biointerfaces 2015, 136, 46–55. [PubMed: 26355812]

38. Marino A; Genchi GG; Sinibaldi E; Ciofani G, Piezoelectric effects of materials on biointerfaces. ACS applied materials & interfaces 2017, 9, 17663–17680. [PubMed: 28485910]

39. Fukada E, Piezoelectricity of wood. Journal of the Physical Society of Japan 1955, 10, 149–154.

40. Fukada E; Sasaki S, Piezoelectricity of α-chitin. Journal of Polymer Science: Polymer Physics Edition 1975, 13, 1845–1847.

41. Fukada E; Yasuda I, On the piezoelectric effect of bone. Journal of the physical society of Japan 1957, 12, 1158–1162.

42. Lemanov V, Piezoelectric and pyroelectric properties of protein amino acids as basic materials of soft state physics. Ferroelectrics 2000, 238, 211–218.

43. Lemanov V; Popov S; Pankova G, Piezoelectric properties of crystals of some protein aminoacids and their related compounds. Physics of the Solid State 2002, 44, 1929–1935.

44. Lemanov V; Popov S, Phonon echo in L-alanine. Physics of the Solid State 1998, 40, 1921–1922.

45. Lemanov V; Popov S, Unusual electromechanical effects in glycine. Physics of the Solid State 1998, 40, 991–994.

46. Lemanov V; Popov S; Pankova G, Piezoelectricity in protein amino acids. Physics of the Solid State 2011, 53, 1191–1193.

47. Heredia A; Meunier V; Bdikin IK; Gracio J; Balke N; Jesse S; Tselev A; Agarwal PK; Sumpter BG; Kalinin SV, Nanoscale ferroelectricity in crystalline γ-glycine. Advanced Functional Materials 2012, 22, 2996–3003.

48. Isakov D; Gomes E. d. M.; Bdikin I; Almeida B; Belsley M; Costa M; Rodrigues V; Heredia A, Production of polar β-glycine nanofibers with enhanced nonlinear optical and piezoelectric properties. Crystal Growth & Design 2011, 11, 4288–4291.

49. Kumar RA; Vizhi RE; Vijayan N; Babu DR, Structural, dielectric and piezoelectric properties of nonlinear optical γ-glycine single crystals. Physica B: Condensed Matter 2011, 406, 2594–2600.

50. Guerin S; Stapleton A; Chovan D; Mouras R; Gleeson M; McKeown C; Noor MR; Silien C; Rhen FM; Kholkin AL, Control of piezoelectricity in amino acids by supramolecular packing. Nature materials 2018, 17, 180. [PubMed: 29200197]

51. Wu J; Xiao D; Zhu J, Potassium–sodium niobate lead-free piezoelectric materials: past, present, and future of phase boundaries. Chemical reviews 2015, 115, 2559–2595. [PubMed: 25792114]

52. Vasilescu D; Cornillon R; Mallet G, Piezoelectric resonances in amino-acids. Nature 1970, 225, 635. [PubMed: 5413369]

53. Guerin S; O'Donnell J; Haq EU; McKeown C; Silien C; Rhen FM; Soulimane T; Tofail SA; Thompson D, Racemic amino acid piezoelectric transducer. Physical review letters 2019, 122, 047701. [PubMed: 30768312]

54. Yan X; Zhu P; Li J, Self-assembly and application of diphenylalanine-based nanostructures. Chemical Society Reviews 2010, 39, 1877–1890. [PubMed: 20502791]

55. Reches M; Gazit E, Casting metal nanowires within discrete self-assembled peptide nanotubes. Science 2003, 300, 625–627. [PubMed: 12714741]

56. Yan X; He Q; Wang K; Duan L; Cui Y; Li J, Transition of cationic dipeptide nanotubes into vesicles and oligonucleotide delivery. Angewandte Chemie International Edition 2007, 46, 2431–2434. [PubMed: 17328086]

57. Anderson J; Lake PT; McCullagh M, Initial Aggregation and Ordering Mechanism of Diphenylalanine from Microsecond All-Atom Molecular Dynamics Simulations. The Journal of Physical Chemistry B 2018, 122, 12331–12341. [PubMed: 30511861]

58. Frederix PW; Ulijn RV; Hunt NT; Tuttle T, Virtual screening for dipeptide aggregation: toward predictive tools for peptide self-assembly. The journal of physical chemistry letters 2011, 2, 2380–2384. [PubMed: 23795243]

59. Guo C; Luo Y; Zhou R; Wei G, Probing the self-assembly mechanism of diphenylalanine-based peptide nanovesicles and nanotubes. ACS nano 2012, 6, 3907–3918. [PubMed: 22468743]

60. Kholkin A; Amdursky N; Bdikin I; Gazit E; Rosenman G, Strong piezoelectricity in bioinspired peptide nanotubes. ACS nano 2010, 4, 610–614. [PubMed: 20131852]

61. Safaryan S; Slabov V; Kopyl S; Romanyuk K; Bdikin I; Vasilev S; Zelenovskiy P; Shur VY; Uslamin EA; Pidko EA, Diphenylalanine-based microribbons for piezoelectric applications via inkjet printing. ACS applied materials & interfaces 2018, 10, 10543–10551. [PubMed: 29498259]

62. Vasilev S; Zelenovskiy P; Vasileva D; Nuraeva A; Shur VY; Kholkin AL, Piezoelectric properties of diphenylalanine microtubes prepared from the solution. Journal of Physics and Chemistry of Solids 2016, 93, 68–72.

63. Nguyen V; Jenkins K; Yang R, Epitaxial growth of vertically aligned piezoelectric diphenylalanine peptide microrods with uniform polarization. Nano Energy 2015, 17, 323–329.

64. Jenkins K; Kelly S; Nguyen V; Wu Y; Yang R, Piezoelectric diphenylalanine peptide for greatly improved flexible nanogenerators. Nano Energy 2018, 51, 317–323.

65. Nguyen V; Zhu R; Jenkins K; Yang R, Self-assembly of diphenylalanine peptide with controlled polarization for power generation. Nature communications 2016, 7, 13566.

66. Stapleton A; Noor M; Sweeney J; Casey V; Kholkin A; Silien C; Gandhi A; Soulimane T; Tofail S, The direct piezoelectric effect in the globular protein lysozyme. Applied Physics Letters 2017, 111, 142902.

67. Kalinin SV; Rodriguez BJ; Jesse S; Seal K; Proksch R; Hohlbauch S; Revenko I; Thompson GL; Vertegel AA, Towards local electromechanical probing of cellular and biomolecular systems in a liquid environment. Nanotechnology 2007, 18, 424020. [PubMed: 21730453]

68. Stapleton A; Noor MR; Haq EU; Silien C; Soulimane T; Tofail SA, Pyroelectricity in globular protein lysozyme films. Journal of Applied Physics 2018, 123, 124701.

69. Wang W; Wu Z; Dai Z; Yang Y; Wang J; Wu G, Glycine metabolism in animals and humans: implications for nutrition and health. Amino acids 2013, 45, 463–477. [PubMed: 23615880]

70. Reitzer L, Catabolism of Amino Acids and Related Compounds. EcoSal Plus 2005, 1.

71. Heredia A; Bdikin I; Kopyl S; Mishina E; Semin S; Sigov A; German K; Bystrov V; Gracio J; Kholkin A, Temperature-driven phase transformation in self-assembled diphenylalanine peptide nanotubes. Journal of Physics D: Applied Physics 2010, 43, 462001.

72. Handelman A; Beker P; Amdursky N; Rosenman G, Physics and engineering of peptide supramolecular nanostructures. Physical Chemistry Chemical Physics 2012, 14, 6391–6408. [PubMed: 22460950]

73. Kol N; Adler-Abramovich L; Barlam D; Shneck RZ; Gazit E; Rousso I, Self-assembled peptide nanotubes are uniquely rigid bioinspired supramolecular structures. Nano letters 2005, 5, 1343–1346. [PubMed: 16178235]

74. Matricardi P; Di Meo C; Coviello T; Hennink WE; Alhaique F, Interpenetrating polymer networks polysaccharide hydrogels for drug delivery and tissue engineering. Advanced Drug Delivery Reviews 2013, 65, 1172–1187. [PubMed: 23603210]

75. Felt O; Buri P; Gurny R, Chitosan: a unique polysaccharide for drug delivery. Drug development and industrial pharmacy 1998, 24, 979–993. [PubMed: 9876553]

76. Azzam T; Eliyahu H; Shapira L; Linial M; Barenholz Y; Domb AJ, Polysaccharide– oligoamine based conjugates for gene delivery. Journal of medicinal chemistry 2002, 45, 1817–1824. [PubMed: 11960493]

77. Khan W; Hosseinkhani H; Ickowicz D; Hong P-D; Yu D-S; Domb AJ, Polysaccharide gene transfection agents. Acta biomaterialia 2012, 8, 4224–4232. [PubMed: 23022542]

78. Janes K; Calvo P; Alonso M, Polysaccharide colloidal particles as delivery systems for macromolecules. Advanced drug delivery reviews 2001, 47, 83–97. [PubMed: 11251247]

79. Suh J-KF; Matthew HW, Application of chitosan-based polysaccharide biomaterials in cartilage tissue engineering: a review. Biomaterials 2000, 21, 2589–2598. [PubMed: 11071608]

80. Moon RJ; Martini A; Nairn J; Simonsen J; Youngblood J, Cellulose nanomaterials review: structure, properties and nanocomposites. Chemical Society Reviews 2011, 40, 3941–3994. [PubMed: 21566801]

81. Wang X; Yao C; Wang F; Li Z, Cellulose-based nanomaterials for energy applications. Small 2017, 13, 1702240.

82. Fukada E, Piezoelectricity as a fundamental property of wood. Wood Science and Technology 1968, 2, 299–307.

83. Bazhenov VA e. Piezoelectric properties of wood; 1961.

84. García Y; Ruiz-Blanco YB; Marrero-Ponce Y; Sotomayor-Torres CM, Orthotropic piezoelectricity in 2D nanocellulose. Scientific reports 2016, 6, 34616. [PubMed: 27708364]

85. Csoka L; Hoeger IC; Rojas OJ; Peszlen I; Pawlak JJ; Peralta PN, Piezoelectric effect of cellulose nanocrystals thin films. ACS Macro Letters 2012, 1, 867–870.

86. Kim J-H; Yun S; Kim J-H; Kim J, Fabrication of piezoelectric cellulose paper and audio application. Journal of Bionic Engineering 2009, 6, 18–21.

87. Kim J; Seo YB, Electro-active paper actuators. Smart Materials and Structures 2002, 11, 355.

88. Kim J; Song C-S; Yun S-R, Cellulose based electro-active papers: performance and environmental effects. Smart Materials and Structures 2006, 15, 719.

89. Kim HS; Li Y; Kim J, Electro-mechanical behavior and direct piezoelectricity of cellulose electro-active paper. Sensors and Actuators A: Physical 2008, 147, 304–309.

90. Chae I; Jeong CK; Ounaies Z; Kim SH, Review on Electromechanical Coupling Properties of Biomaterials. ACS Applied Bio Materials 2018, 1, 936–953.

91. Kumar MNR, A review of chitin and chitosan applications. Reactive and functional polymers 2000, 46, 1–27.

92. Jardine A; Sayed S, Challenges in the valorisation of chitinous biomass within the biorefinery concept. Current Opinion in Green and Sustainable Chemistry 2016, 2, 34–39.

93. Kim K; Ha M; Choi B; Joo SH; Kang HS; Park JH; Gu B; Park C; Park C; Kim J, Biodegradable, electro-active chitin nanofiber films for flexible piezoelectric transducers. Nano Energy 2018, 48, 275–283.

94. Béguin P; Aubert J-P, The biological degradation of cellulose. FEMS microbiology reviews 1994, 13, 25–58. [PubMed: 8117466]

95. Helenius G; Bäckdahl H; Bodin A; Nannmark U; Gatenholm P; Risberg B, In vivo biocompatibility of bacterial cellulose. Journal of Biomedical Materials Research Part A: An Official Journal of The Society for Biomaterials, The Japanese Society for Biomaterials, and The Australian Society for Biomaterials and the Korean Society for Biomaterials 2006, 76, 431–438.

96. Haigler CH; White AR; Brown RM; Cooper KM, Alteration of in vivo cellulose ribbon assembly by carboxymethylcellulose and other cellulose derivatives. The Journal of cell biology 1982, 94, 64–69. [PubMed: 6889605]

97. Fricain J; Granja P; Barbosa M; De Jéso B; Barthe N; Baquey C, Cellulose phosphates as biomaterials. In vivo biocompatibility studies. Biomaterials 2002, 23, 971–980. [PubMed: 11791931]

98. Dimitrijevich SD; Tatarko M; Gracy RW; Wise GE; Oakford LX; Linsky CB; Kamp L, In vivo degradation of oxidized, regenerated cellulose. Carbohydrate research 1990, 198, 331–341. [PubMed: 2379193]

99. Tomihata K; Ikada Y, In vitro and in vivo degradation of films of chitin and its deacetylated derivatives. Biomaterials 1997, 18, 567–575. [PubMed: 9105597]

100. Sashiwa H; Saimoto H; Shigemasa Y; Ogawa R; Tokura S, Lysozyme susceptibility of partially deacetylated chitin. International journal of biological macromolecules 1990, 12, 295–296. [PubMed: 2085495]

101. Pangburn S; Trescony P; Heller J, Lysozyme degradation of partially deacetylated chitin, its films and hydrogels. Biomaterials 1982, 3, 105–108. [PubMed: 7082736]

102. Lang SB, Pyroelectric effect in bone and tendon. Nature 1966, 212, 704.

103. Marino AA; Becker RO; Soderholm SC, Origin of the piezoelectric effect in bone. Calcified tissue research 1971, 8, 177–180. [PubMed: 5145213]

104. Volkov V; Ferreira AV; Cavaco - Paulo A, On the Routines of Wild - Type Silk Fibroin Processing Toward Silk-Inspired Materials: A Review. Macromolecular Materials and Engineering 2015, 300, 1199–1216.

105. Vepari C; Kaplan DL, Silk as a biomaterial. Progress in polymer science 2007, 32, 991–1007. [PubMed: 19543442]

106. Fukada E, On the piezoelectric effect of silk fibers. Journal of the Physical Society of Japan 1956, 11, 1301A–1301A.

107. Yucel T; Cebe P; Kaplan DL, Structural origins of silk piezoelectricity. Advanced functional materials 2011, 21, 779–785. [PubMed: 23335872]

108. Jesse S; Mirman B; Kalinin SV, Resonance enhancement in piezoresponse force microscopy: Mapping electromechanical activity, contact stiffness, and Q factor. Applied physics letters 2006, 89, 022906.

109. Seol D; Kim B; Kim Y, Non-piezoelectric effects in piezoresponse force microscopy. Current Applied Physics 2017, 17, 661–674.

110. Pan C-T; Yen C-K; Hsieh M-C; Wang S-Y; Chien C-H; Huang JC-C; Lin L; Shiue Y-L; Kuo S-W, Energy Harvesters Incorporating Silk from the Taiwan-Native Spider Nephila pilipes. ACS Applied Energy Materials 2018, 1, 5627–5635.

111. Zhang Y; Gandhi A; Zeglinski J; Gregor M; Tofail S, A complementary contribution to piezoelectricity from bone constituents. IEEE Transactions on Dielectrics and Electrical Insulation 2012, 19, 1151–1157.

112. Lang S; Tofail S; Kholkin A; Wojta M; Gregor M; Gandhi A; Wang Y; Bauer S; Krause M; Plecenik A, Ferroelectric polarization in nanocrystalline hydroxyapatite thin films on silicon. Scientific reports 2013, 3, 2215. [PubMed: 23884324]

113. Lang S; Tofail S; Gandhi A; Gregor M; Wolf-Brandstetter C; Kost J; Bauer S; Krause M, Pyroelectric, piezoelectric, and photoeffects in hydroxyapatite thin films on silicon. Applied physics letters 2011, 98, 123703.

114. Ravi HK; Simona F; Hulliger J. r.; Cascella M, Molecular Origin of Piezo-and Pyroelectric Properties in Collagen Investigated by Molecular Dynamics Simulations. The Journal of Physical Chemistry B 2012, 116, 1901–1907. [PubMed: 22242946]

115. Zhou Z; Qian D; Minary-Jolandan M, Molecular mechanism of polarization and piezoelectric effect in super-twisted collagen. ACS Biomaterials Science & Engineering 2016, 2, 929–936.

116. Ricard-Blum S, The collagen family. Cold Spring Harbor perspectives in biology 2011, 3, a004978. [PubMed: 21421911]

117. Cen L; Liu W; Cui L; Zhang W; Cao Y, Collagen tissue engineering: development of novel biomaterials and applications. Pediatric research 2008, 63, 492. [PubMed: 18427293]

118. Denning D; Kilpatrick JI; Fukada E; Zhang N; Habelitz S; Fertala A; Gilchrist MD; Zhang Y; Tofail SA; Rodriguez BJ, Piezoelectric Tensor of Collagen Fibrils Determined at the Nanoscale. ACS Biomaterials Science & Engineering 2017, 3, 929–935.

119. Levin LA; Albert DM, Ocular Disease: Mechanisms and Management E-Book: Expert Consult-Online and Print. Elsevier Health Sciences: 2010.

120. Ghosh S; Mei B; Lubkin V; Scheinbeim J; Newman B; Kramer P; Bennett G; Feit N, Piezoelectric response of scleral collagen. Journal of Biomedical Materials Research: An Official Journal of The Society for Biomaterials, The Japanese Society for Biomaterials, and the Australian Society for Biomaterials 1998, 39, 453–457.

121. Denning D; Kilpatrick J; Hsu T; Habelitz S; Fertala A; Rodriguez B, Piezoelectricity in collagen type II fibrils measured by scanning probe microscopy. Journal of Applied Physics 2014, 116, 066818.

122. Cao Y; Wang B, Biodegradation of silk biomaterials. International journal of molecular sciences 2009, 10, 1514–1524. [PubMed: 19468322]

123. Numata K; Cebe P; Kaplan DL, Mechanism of enzymatic degradation of beta-sheet crystals. Biomaterials 2010, 31, 2926–2933. [PubMed: 20044136]

124. Horan RL; Antle K; Collette AL; Wang Y; Huang J; Moreau JE; Volloch V; Kaplan DL; Altman GH, In vitro degradation of silk fibroin. Biomaterials 2005, 26, 3385–3393. [PubMed: 15621227]

125. Minoura N; Tsukada M; Nagura M, Physico-chemical properties of silk fibroin membrane as a biomaterial. Biomaterials 1990, 11, 430–434. [PubMed: 2207234]

126. Li M; Ogiso M; Minoura N, Enzymatic degradation behavior of porous silk fibroin sheets. Biomaterials 2003, 24, 357–365. [PubMed: 12419638]

127. Wang Y; Rudym DD; Walsh A; Abrahamsen L; Kim H-J; Kim HS; Kirker-Head C; Kaplan DL, In vivo degradation of three-dimensional silk fibroin scaffolds. Biomaterials 2008, 29, 3415–3428. [PubMed: 18502501]

128. Laurent G, Dynamic state of collagen: pathways of collagen degradation in vivo and their possible role in regulation of collagen mass. American Journal of Physiology-Cell Physiology 1987, 252, C1–C9.

129. Alberti KA; Xu Q, Biocompatibility and degradation of tendon-derived scaffolds. Regenerative biomaterials 2015, 3, 1–11. [PubMed: 26816651]

130. Lodish H; Berk A; Zipursky SL; Matsudaira P; Baltimore D; Darnell J, Viruses: structure, function, and uses In Molecular Cell Biology. 4th edition, WH Freeman: 2000.

131. Giacca M; Zacchigna S, Virus-mediated gene delivery for human gene therapy. Journal of controlled release 2012, 161, 377–388. [PubMed: 22516095]

132. Dalkara D; Byrne LC; Klimczak RR; Visel M; Yin L; Merigan WH; Flannery JG; Schaffer DV, In vivo–directed evolution of a new adeno-associated virus for therapeutic outer retinal gene delivery from the vitreous. Science translational medicine 2013, 5, 189ra76–189ra76.

133. Lee BY; Zhang J; Zueger C; Chung W-J; Yoo SY; Wang E; Meyer J; Ramesh R; Lee S-W, Virus-based piezoelectric energy generation. Nature nanotechnology 2012, 7, 351.

134. Lee J-H; Lee JH; Xiao J; Desai MS; Zhang X; Lee S-W, Vertical Self-Assembly of Polarized Phage Nanostructure for Energy Harvesting. Nano letters 2019, 19, 2661–2667. [PubMed: 30875472]

135. Shin D-M; Han HJ; Kim W-G; Kim E; Kim C; Hong SW; Kim HK; Oh J-W; Hwang Y-H, Bioinspired piezoelectric nanogenerators based on vertically aligned phage nanopillars. Energy & Environmental Science 2015, 8, 3198–3203.

136. Chung W-J; Lee D-Y; Yoo SY, Chemical modulation of M13 bacteriophage and its functional opportunities for nanomedicine. International journal of nanomedicine 2014, 9, 5825. [PubMed: 25540583]

137. Tóthová L. u.; Bábí ková J; Celec P, Phage survival: the biodegradability of M13 phage display library in vitro. Biotechnology and applied biochemistry 2012, 59, 490–494. [PubMed: 23586959]

138. Garlotta D, A literature review of poly (lactic acid). Journal of Polymers and the Environment 2001, 9, 63–84.

139. Rasal RM; Janorkar AV; Hirt DE, Poly (lactic acid) modifications. Progress in polymer science 2010, 35, 338–356.

140. Tokiwa Y; Calabia BP, Biodegradability and biodegradation of poly (lactide). Applied microbiology and biotechnology 2006, 72, 244–251. [PubMed: 16823551]

141. Lee SJ; Arun AP; Kim KJ, Piezoelectric properties of electrospun poly (l-lactic acid) nanofiber web. Materials letters 2015, 148, 58–62.

142. Ando M; Takeshima S; Ishiura Y; Ando K; Onishi O, Piezoelectric antibacterial fabric comprised of poly (l-lactic acid) yarn. Japanese Journal of Applied Physics 2017, 56, 10PG01.

143. Ando M; Kawamura H; Kitada H; Sekimoto Y; Inoue T; Tajitsu Y, Pressure-sensitive touch panel based on piezoelectric poly (L-lactic acid) film. Japanese Journal of Applied Physics 2013, 52, 09KD17.

144. Ando M; Kawamura H; Kitada H; Sekimoto Y; Inoue T; Tajitsu Y In New human machine interface devices using a piezoelectric poly (L-lactic acid) film, 2013 Joint IEEE International Symposium on Applications of Ferroelectric and Workshop on Piezoresponse Force Microscopy (ISAF/PFM), IEEE: 2013; pp 236–239.

145. Ochiai T; Fukada E, Electromechanical properties of poly-L-lactic acid. Japanese journal of applied physics 1998, 37, 3374.

146. Curry EJ; Ke K; Chorsi MT; Wrobel KS; Miller AN; Patel A; Kim I; Feng J; Yue L; Wu Q, Biodegradable piezoelectric force sensor. Proceedings of the National Academy of Sciences 2018, 115, 909–914.

147. Smith M; Calahorra Y; Jing Q; Kar-Narayan S, Direct observation of shear piezoelectricity in poly-l-lactic acid nanowires. APL Materials 2017, 5, 074105.

148. Sencadas V; Ribeiro C; Heredia A; Bdikin I; Kholkin AL; Lanceros-Méndez S, Local piezoelectric activity of single poly (L-lactic acid)(PLLA) microfibers. Applied Physics A 2012, 109, 51–55.

149. Walton M; Cotton NJ, Long-term in vivo degradation of poly-L-lactide (PLLA) in bone. Journal of biomaterials applications 2007, 21, 395–411. [PubMed: 16684797]

150. Laitinen O; Törmälä P; Taurio R; Skutnabb K; Saarelainen K; Iivonen T; Vainionpää S, Mechanical properties of biodegradable ligament augmentation device of poly (L-lactide) in vitro and in vivo. Biomaterials 1992, 13, 1012–1016. [PubMed: 1472587]

151. Pistner H; Bendi DR; Mühling J; Reuther JF, Poly (l-lactide): a long-term degradation study in vivo: Part III. Analytical characterization. Biomaterials 1993, 14, 291–298. [PubMed: 8476999]

152. Bos R; Rozema F; Boering G; Nijenhius A; Pennings A; Verwey A; Nieuwenhuis P; Jansen H, Degradation of and tissue reaction to biodegradable poly (L-lactide) for use as internal fixation of fractures: a study in rats. Biomaterials 1991, 12, 32–36. [PubMed: 2009343]

153. Bergsma JE; De Bruijn W; Rozema F; Bos R; Boering G, Late degradation tissue response to poly (L-lactide) bone plates and screws. Biomaterials 1995, 16, 25–31. [PubMed: 7718688]

154. Nicolini C, From neural chip and engineered biomolecules to bioelectronic devices: an overview. Biosensors and Bioelectronics 1995, 10, 105–127. [PubMed: 7734117]

155. Zhang A; Lieber CM, Nano-bioelectronics. Chemical reviews 2015, 116, 215–257. [PubMed: 26691648]

156. Yuk H; Lu B; Zhao X, Hydrogel bioelectronics. Chemical Society Reviews 2019, 48, 1642–1667. [PubMed: 30474663]

157. Koo J; MacEwan MR; Kang S-K; Won SM; Stephen M; Gamble P; Xie Z; Yan Y; Chen Y-Y; Shin J, Wireless bioresorbable electronic system enables sustained nonpharmacological neuroregenerative therapy. Nature medicine 2018, 24, 1830.

158. Guo Q; Koo J; Xie Z; Avila R; Yu X; Ning X; Zhang H; Liang X; Kim SB; Yan Y, A Bioresorbable Magnetically Coupled System for Low - Frequency Wireless Power Transfer. Advanced Functional Materials 2019, 1905451.

159. Someya T; Bao Z; Malliaras GG, The rise of plastic bioelectronics. Nature 2016, 540, 379. [PubMed: 27974769]

160. Boutry CM; Beker L; Kaizawa Y; Vassos C; Tran H; Hinckley AC; Pfattner R; Niu S; Li J; Claverie J, Biodegradable and flexible arterial-pulse sensor for the wireless monitoring of blood flow. Nature biomedical engineering 2019, 3, 47.

161. Boutry CM; Nguyen A; Lawal QO; Chortos A; Rondeau-Gagné S; Bao Z, A sensitive and biodegradable pressure sensor array for cardiovascular monitoring. Advanced Materials 2015, 27, 6954–6961. [PubMed: 26418964]

162. Li J; Kang L; Yu Y; Long Y; Jeffery JJ; Cai W; Wang X, Study of long-term biocompatibility and bio-safety of implantable nanogenerators. Nano energy 2018, 51, 728–735. [PubMed: 30221128]

163. Lee J-H; Heo K; Schulz-Schönhagen K; Lee JH; Desai MS; Jin H-E; Lee S-W, Diphenylalanine peptide nanotube energy harvesters. ACS nano 2018, 12, 8138–8144. [PubMed: 30071165]

164. Donelan JM; Li Q; Naing V; Hoffer J; Weber D; Kuo AD, Biomechanical energy harvesting: generating electricity during walking with minimal user effort. Science 2008, 319, 807–810. [PubMed: 18258914]

165. Beeby SP; Torah R; Tudor M; Glynne-Jones P; O'donnell T; Saha C; Roy S, A micro electromagnetic generator for vibration energy harvesting. Journal of Micromechanics and microengineering 2007, 17, 1257.

166. Saha C; O'donnell T; Wang N; McCloskey P, Electromagnetic generator for harvesting energy from human motion. Sensors and Actuators A: Physical 2008, 147, 248–253.

167. Long Y; Wei H; Li J; Yao G; Yu B; Ni D; Gibson AL; Lan X; Jiang Y; Cai W, Effective Wound Healing Enabled by Discrete Alternative Electric Fields from Wearable Nanogenerators. ACS nano 2018, 12, 12533–12540. [PubMed: 30488695]

168. Li J; Kang L; Long Y; Wei H; Yu Y; Wang Y; Ferreira CA; Yao G; Zhang Z; Carlos C, Implanted Battery-Free Direct-Current Micro-Power Supply from in Vivo Breath Energy Harvesting. ACS applied materials & interfaces 2018, 10, 42030–42038. [PubMed: 30444344]

169. Wang M; Zhang J; Tang Y; Li J; Zhang B; Liang E; Mao Y; Wang X, Air-flow-driven triboelectric nanogenerators for self-powered real-time respiratory monitoring. ACS nano 2018, 12, 6156–6162. [PubMed: 29847095]

170. Long Y; Yu Y; Yin X; Li J; Carlos C; Du X; Jiang Y; Wang X, Effective anti-biofouling enabled by surface electric disturbance from water wave-driven nanogenerator. Nano energy 2019, 57, 558–565. [PubMed: 30984531]

171. Tajitsu Y; Kawai S; Kanesaki M; Date M; Fukada E, Microactuators with piezoelectric polylactic acid fibers—toward the realization of tweezers for biological cells. Ferroelectrics 2004, 304, 195–200.

172. Tajitsu Y; Kanesaki M; Tsukiji M; Imoto K; Date M; Fukada E, Novel tweezers for biological cells using piezoelectric polylactic acid fibers. Ferroelectrics 2005, 320, 133–139.

173. Tajitsu Y, Development of electric control catheter and tweezers for thrombosis sample in blood vessels using piezoelectric polymeric fibers. Polymers for advanced technologies 2006, 17, 907–913.

174. Ishii D; Ying TH; Mahara A; Murakami S; Yamaoka T; Lee W.-k.; Iwata T, In vivo tissue response and degradation behavior of PLLA and stereocomplexed PLA nanofibers. Biomacromolecules 2008, 10, 237–242.

175. Zhang Q; Mochalin VN; Neitzel I; Knoke IY; Han J; Klug CA; Zhou JG; Lelkes PI; Gogotsi Y, Fluorescent PLLA-nanodiamond composites for bone tissue engineering. Biomaterials 2011, 32, 87–94. [PubMed: 20869765]

176. Martin O; Averous L, Poly (lactic acid): plasticization and properties of biodegradable multiphase systems. Polymer 2001, 42, 6209–6219.

177. Grant CA; Brockwell DJ; Radford SE; Thomson NH, Tuning the elastic modulus of hydrated collagen fibrils. Biophysical journal 2009, 97, 2985–2992. [PubMed: 19948128]

178. Graham JS; Vomund AN; Phillips CL; Grandbois M, Structural changes in human type I collagen fibrils investigated by force spectroscopy. Experimental cell research 2004, 299, 335–342. [PubMed: 15350533]

179. Nakafuku C; Takehisa S. y., Glass transition and mechanical properties of PLLA and PDLLA-PGA copolymer blends. Journal of applied polymer science 2004, 93, 2164–2173.

180. Yasuniwa M; Tsubakihara S; Sugimoto Y; Nakafuku C, Thermal analysis of the double - melting behavior of poly (L-lactic acid). Journal of Polymer Science Part B: Polymer Physics 2004, 42, 25–32.

181. Cui H; Hensleigh R; Yao D; Maurya D; Kumar P; Kang MG; Priya S; Zheng XR, Three-dimensional printing of piezoelectric materials with designed anisotropy and directional response. Nature materials 2019, 18, 234. [PubMed: 30664695]

182. Kim K; Zhu W; Qu X; Aaronson C; McCall WR; Chen S; Sirbuly DJ, 3D optical printing of piezoelectric nanoparticle–polymer composite materials. ACS nano 2014, 8, 9799–9806. [PubMed: 25046646]

183. Shepelin NA; Lussini VC; Fox PJ; Dicinoski GW; Glushenkov AM; Shapter JG; Ellis AV, 3D printing of poly (vinylidene fluoride-trifluoroethylene): a poling-free technique to manufacture flexible and transparent piezoelectric generators. MRS Communications 2019, 9, 159–164.

Highlights

- An overview of the most recent major advancements in novel biodegradable piezoelectric materials was provided for the first time.

- Attempts to decipher origin of piezoelectricity among natural/synthetic materials at molecular scale were introduced.

- In vivo and in vitro disintegration behaviors of novel piezoelectric materials are discussed and analyzed.

- Implementations of biodegradable piezoelectric materials in next-generation bioelectronics (mostly energy harvester/sensor/actuator) are exemplified.

- Challenges toward practical applications together with potential research directions in this field are well summarized.
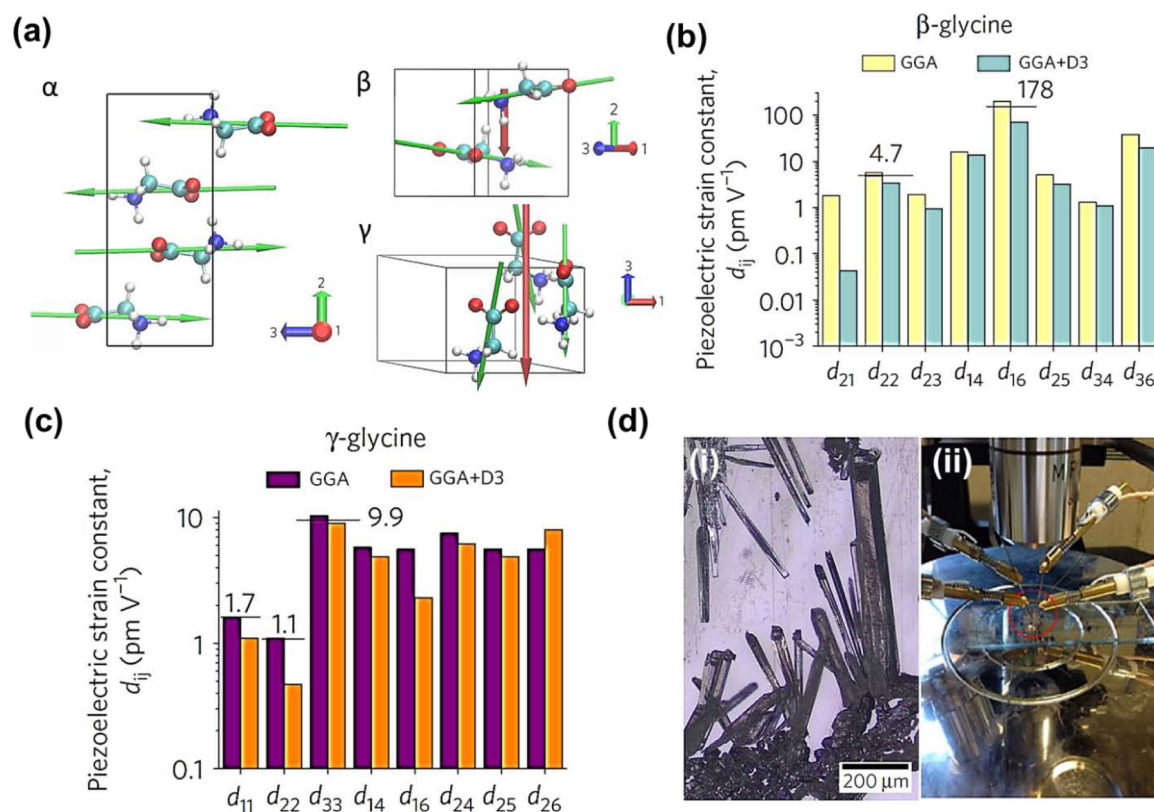
Figure 1.
(a) Computed molecular dipoles in glycine molecules with different polymorphs (α, β, and γ). (b) Calculated piezoelectric coefficients for β -glycine. (c) Calculated piezoelectric coefficients for γ -glycine. (d) (i) As-grown β -glycine microneedles. (ii) Four-point probe electrode set-up for β -glycine piezoresponse measurement. Reprinted with permission from ref 50. Copyright 2018 Springer Nature.
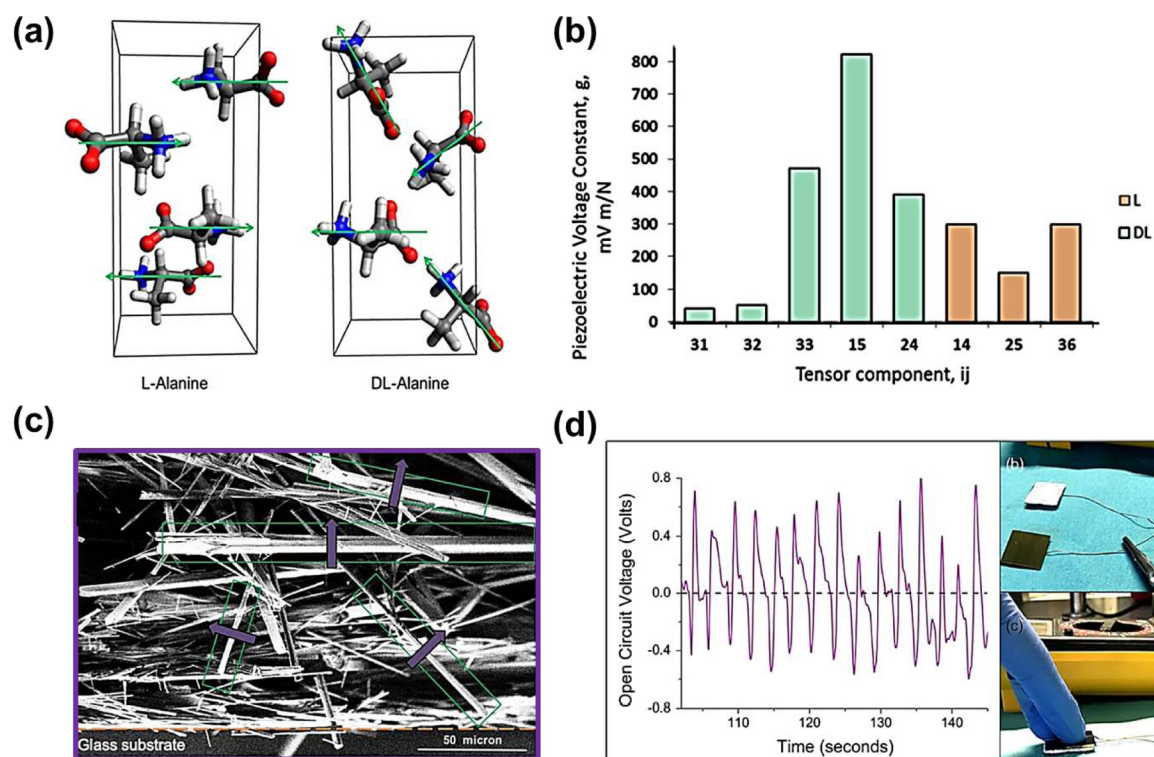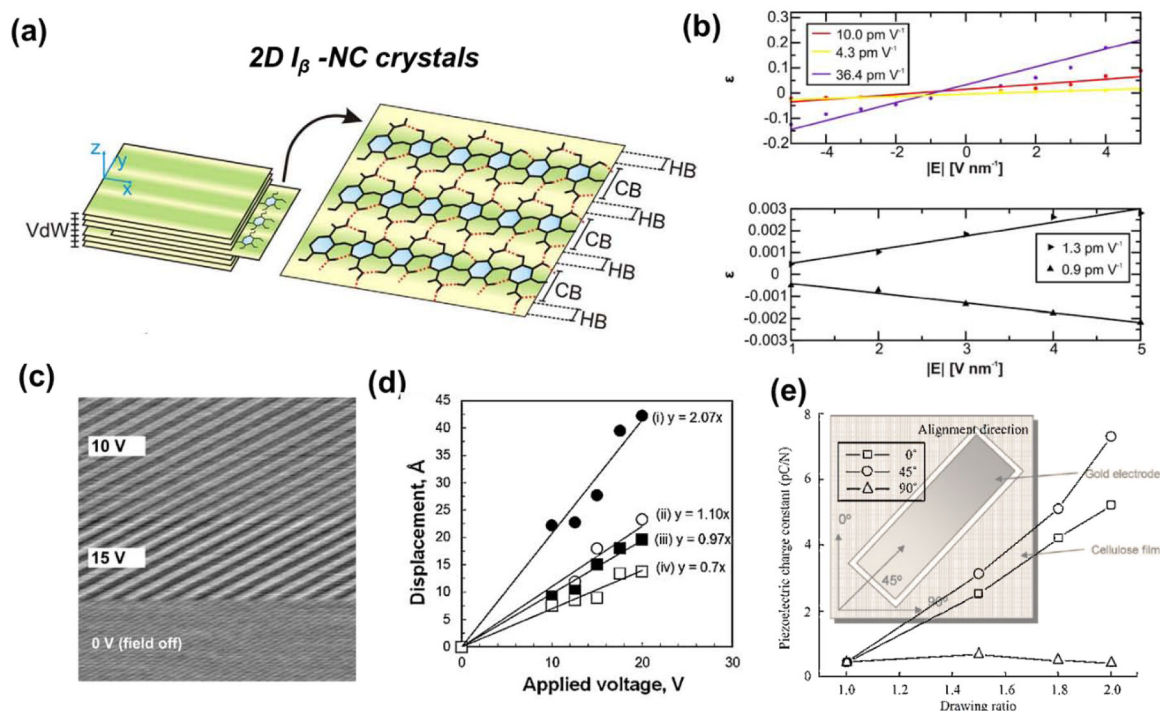
Figure 2.
(a) Molecular dipoles in L-Alanine and DL-Alanine. (b) Calculated piezoelectric voltage coefficients for L-Alanine and DL-Alanine. (c) As-grown racemic DL-Alanine microneedles (d) Open circuit voltage harvested from DL-alanine films under normal finger compression. Reprinted with permission from ref 53. Copyright 2018, the American Physical Society.
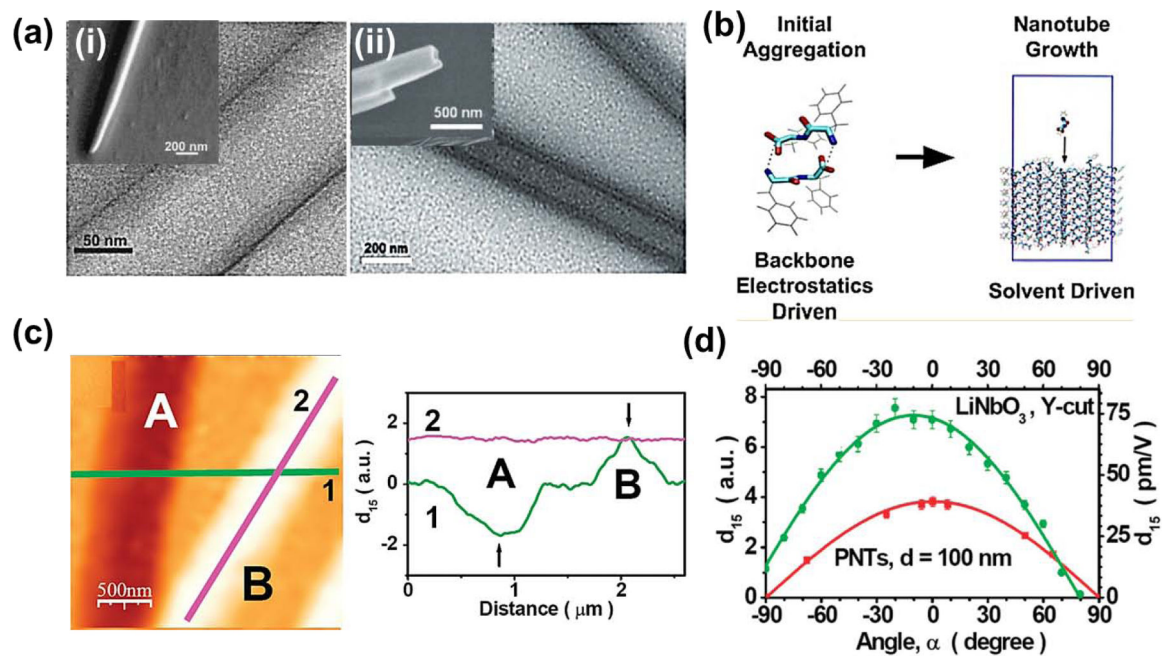
Figure 3.
(a) HR-TEM images of FF peptide nanotubes. Insets are SEM image of individual FF nanotube. (i) Reprinted with permission from ref 55. Copyright 2003, the American Association for the Advancement of Science. (ii) Reprinted with permission from ref 56. Copyright 2007, Wiley-VC. **(b)** Nanotube forming mechanism with initial aggregation and later crystal growth based on molecular dynamic simulation. Reprinted with permission from ref 57. Copyright 2018, the American Chemical Society. **(c)** Piezoelectricity of two nanotubes (A and B) with opposite polarizations. **(d)** Piezoresponses as a function of angle for FF nanotube and Y-cut $LiNbO_3$. Reprinted with permission from ref 60. Copyright 2010, the American Chemical Society
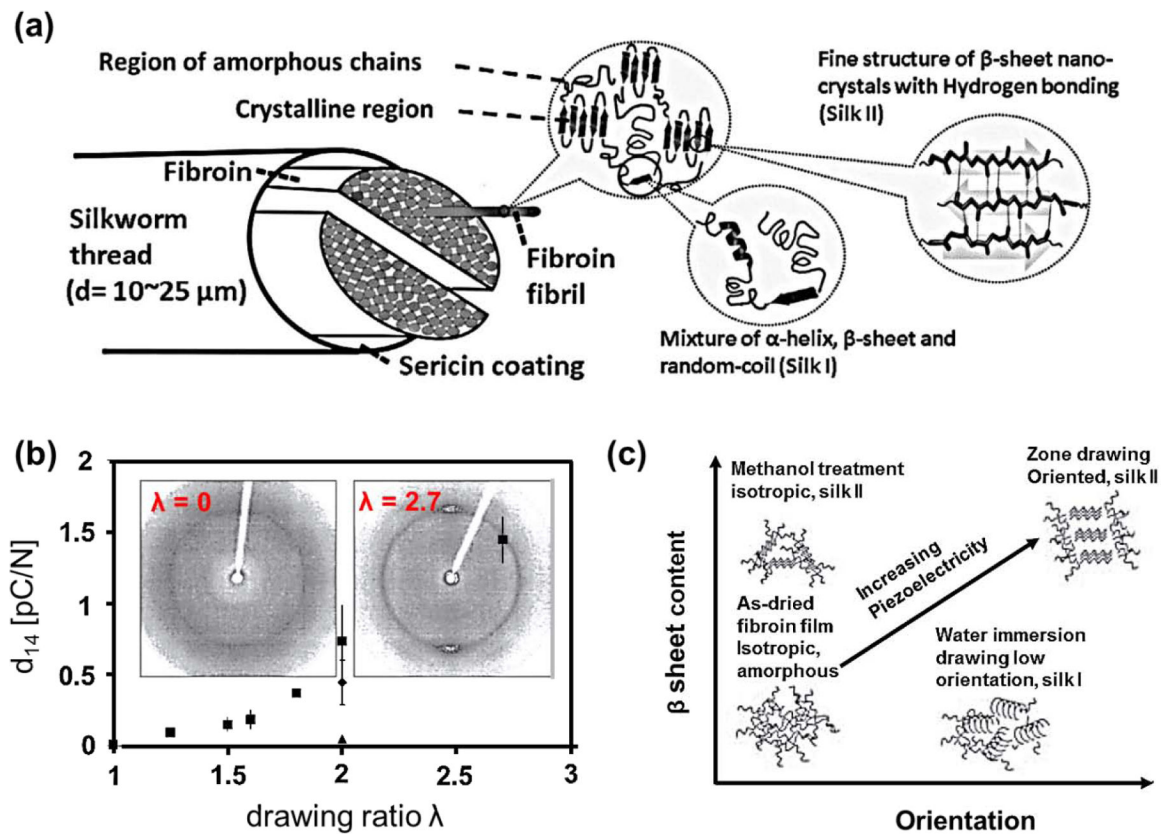
Figure 4.
(a) Schematics of hydrogen and covalent bonding in Quasi-2D nanocellulose slabs stacked by Van der Waals interactions **(b)** calculated piezoelectricity of three single hydrogen bondings (upper panel) and extended crystal (lower panel, d_{22} and d_{11}). Reprinted with permission from ref 84. Copyright 2016, Springer Nature. **(c)** The displacement (z-direction) of cellulose nanocrystal (CNC) film as a result of their piezoelectric effect. **(d)** Vertical displacement of CNC films as a function of applied electric fields. Reprinted with permission from ref 85. Copyright 2010, the American Chemical Society. **(e)** Piezoelectric coefficient of electroactive cellulose paper as a function of the drawing ratio. Reprinted with permission from ref 86. Copyright 2009, Elsevier.
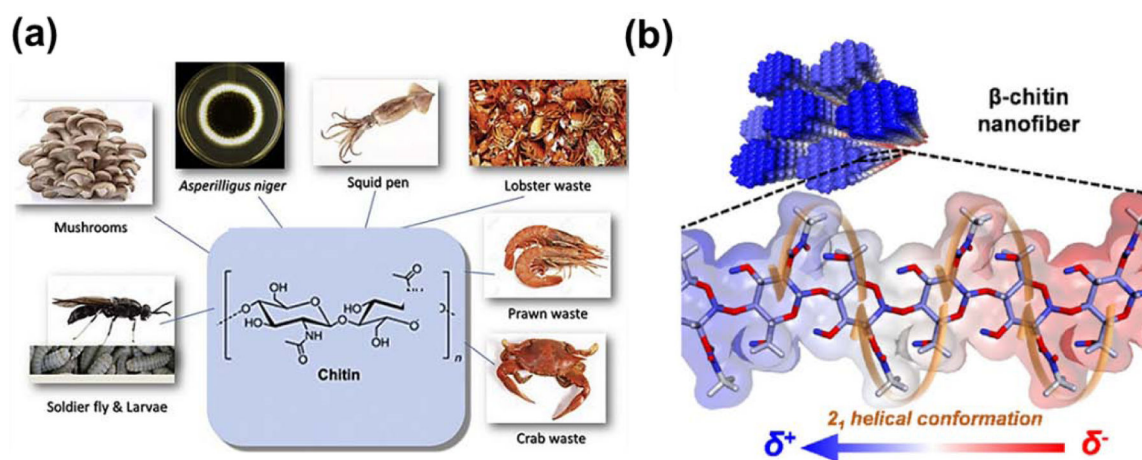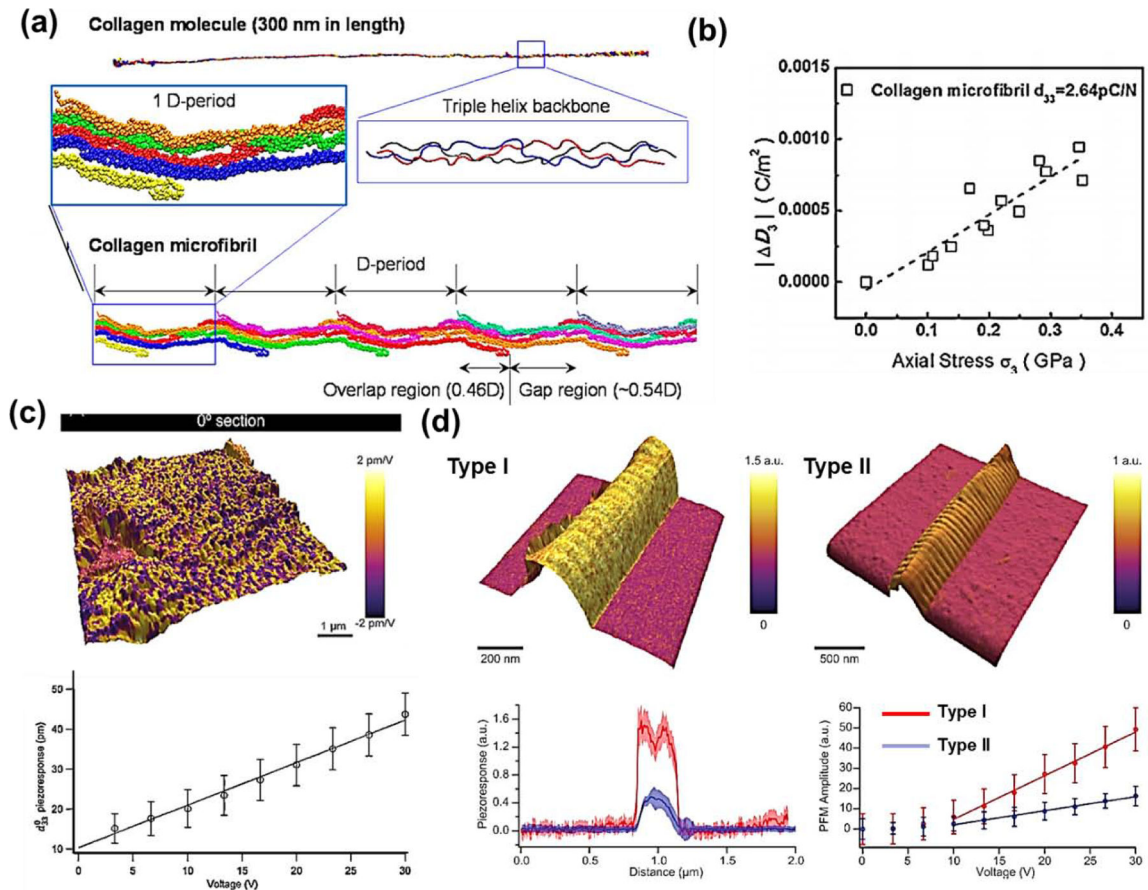
Figure 5.
(a) Chitin as building block that strengthens the exoskeletons and cell walls for many creatures. Reprinted with permission from ref 92. Copyright 2016, Elsevier. (b) DFT simulation of polarizations in β-chitin nanofiber. Reprinted with permission from ref 93. Copyright 2018, Elsevier.
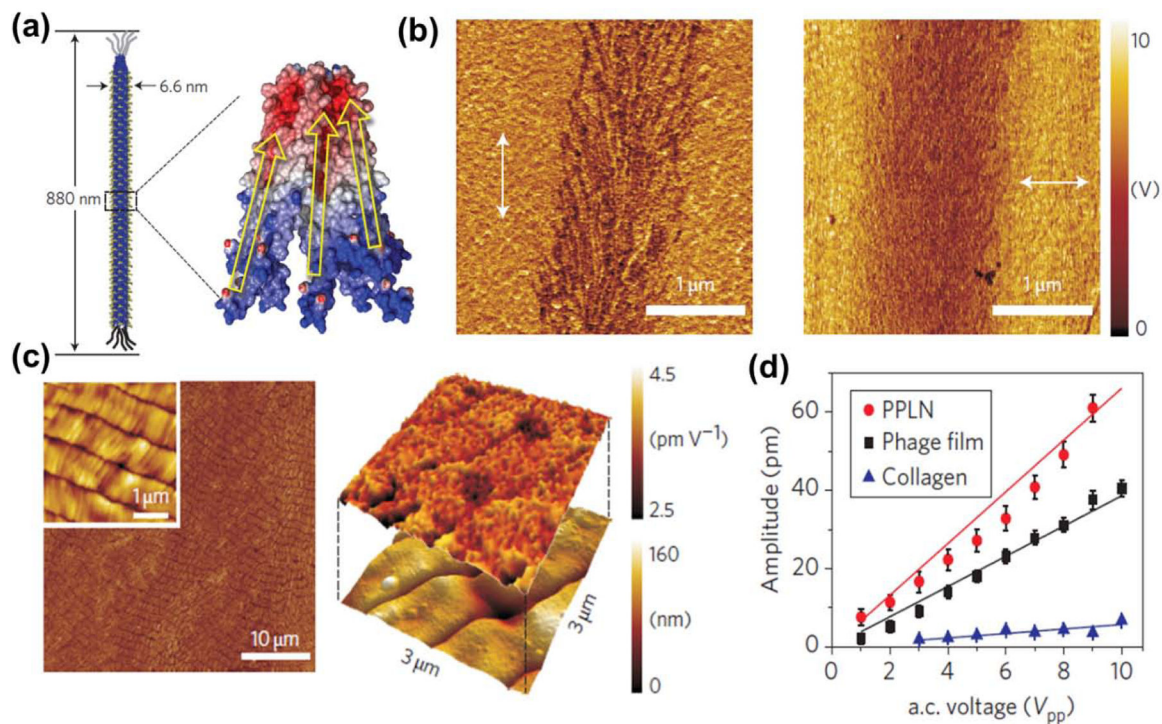
Figure 6.
(a) Schematic image of the deduced silk fibroin structure. Reprinted with permission from ref 104. Copyright 2015, Wiley-VC **(b)** The shear piezoelectric coefficient d_{14} as a function of the drawing ratio λ. Insets are 2D WAXD plots. **(c)** The impact of processing parameters and structure om piezoelectricity in silk fibroin. Reprinted with permission from ref 107. Copyright 2011, Wiley-VC
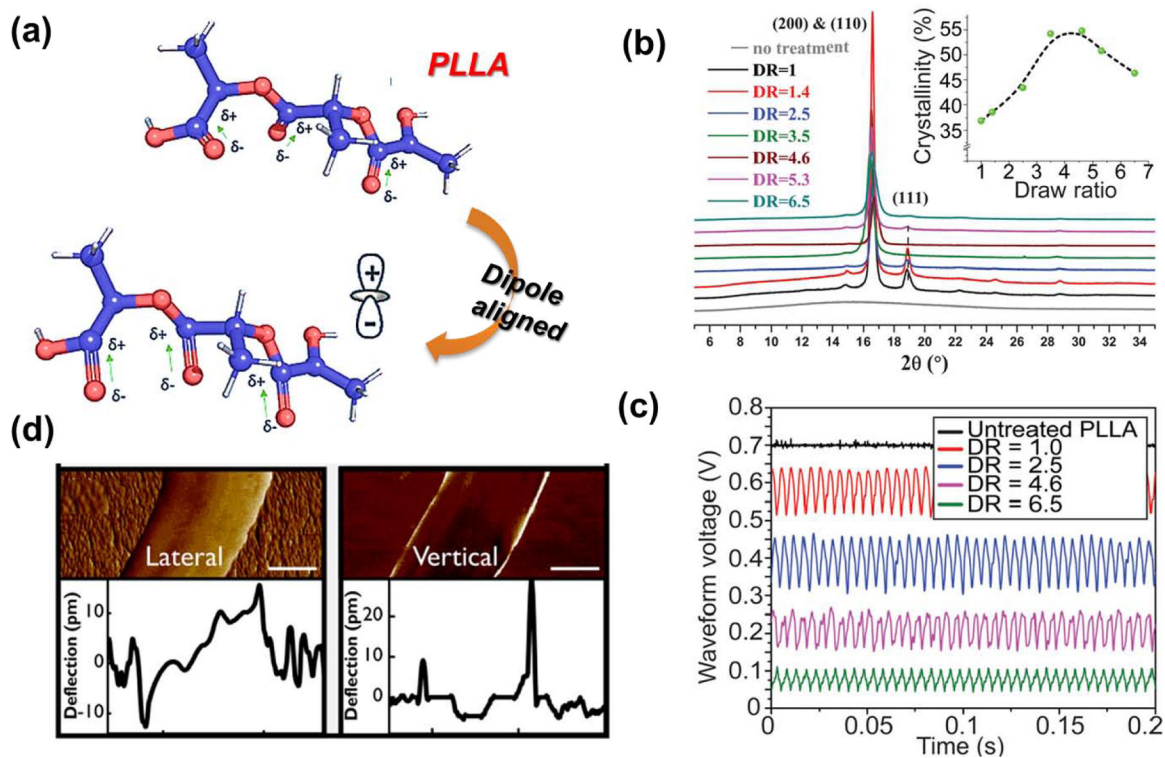
Figure 7.
(a) Simulation models of collagen molecule and collagen microfibril. **(b)** The electric displacement (among z-direction) as a function of axial stress. Reprinted with permission from ref 115. Copyright 2016, the American Chemical Society. **(c)** PFM maps (upper panel) of 0° sections of rat tail tendon and piezoelectric responses in the 0° section (lower panel). Reprinted with permission from ref 118. Copyright 2017, the American Chemical Society. **(d)** AFM topography image of type I and type II collagen fibrils overlaid with piezoresponses (upper panel) and PFM amplitude as a function of AC voltage (lower panel). Reprinted with permission from ref 121. Copyright 2014, the American Institute of Physics Publishing LLC.
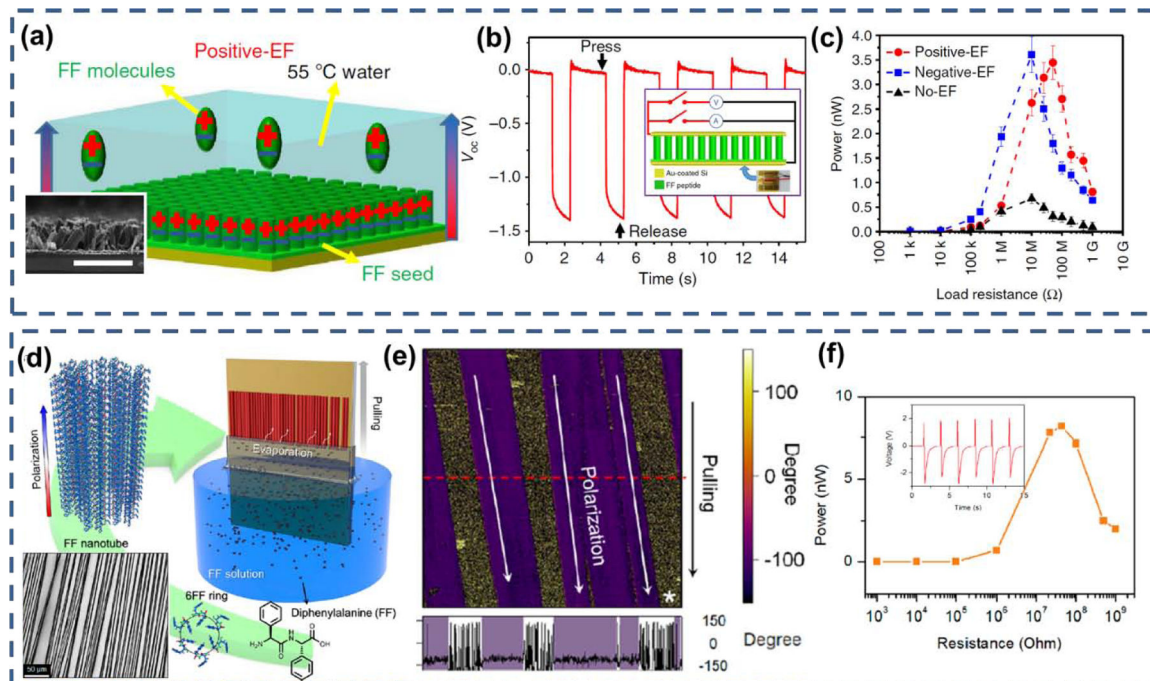
Figure 8.
(a) Schematic of structure and dipole in the M13 phage. **(b)** Lateral PFM image of the monolayer phage film. **(c)** Piezoelectric properties of multilayer 4E-phage films. **(d)** The piezoresponse comparison of 4E-phage films with periodically poled lithium niobate (PPLN) and type I collagen films Reprinted with permission from ref 133. Copyright 2012, Springer Nature.
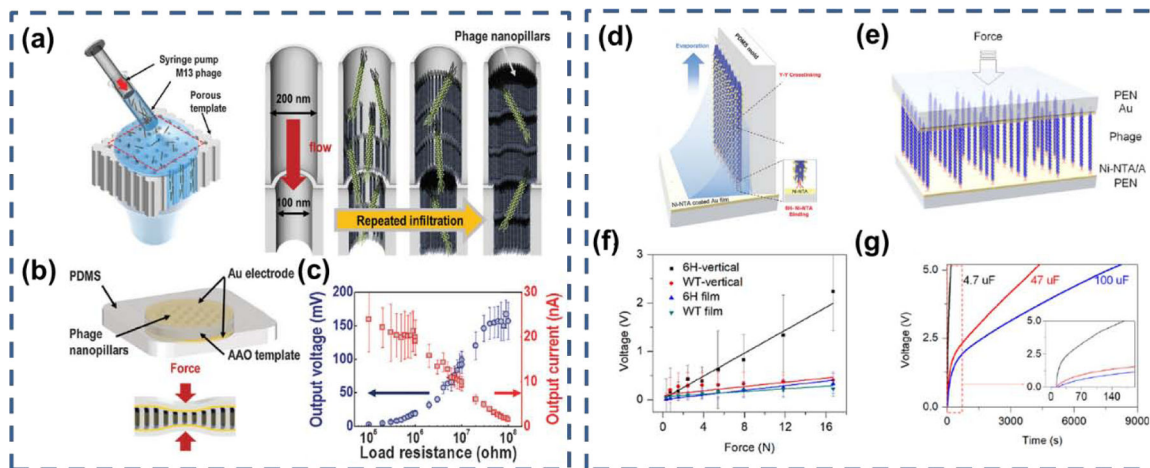
Figure 9.
(a) The schematic of PLLA dipole alignment. **(b)** XRD pattern of PLLA films with different drawing ratio. **(c)** Piezoresponse comparison of PLLA films with different drawing ratio. Reprinted with permission from ref 146. Copyright 2017, National Academy of Sciences.**(d)** Lateral and vertical PFM measurement of individual PLLA nanowire. Reprinted with permission from ref 147. Copyright 2017, the American Institute of Physics Publishing LLC.
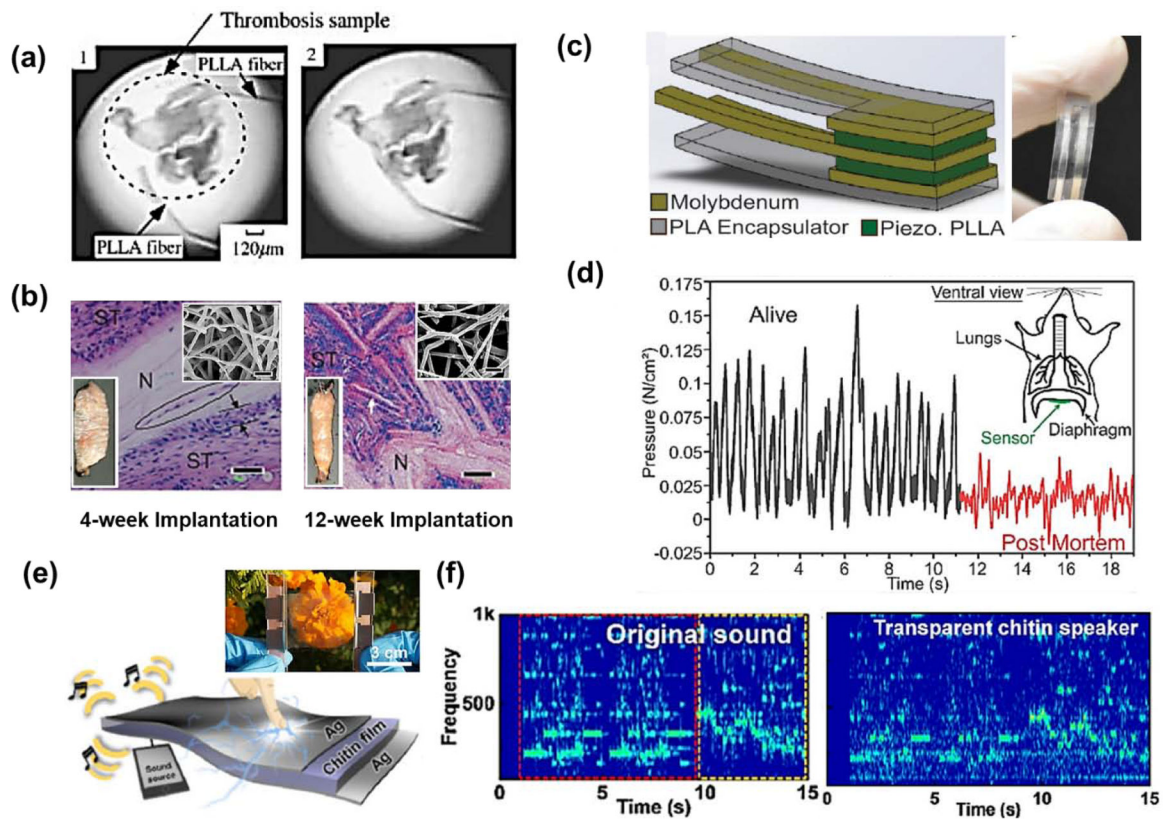
Figure 10.
(a) The schematic of FF microtube growth under electrical field. **(b)** V_{oc} of as-prepared FF energy harvester driven by compression. **(c)** Power output of FF energy harvester as a function of load resistance. Reprinted with permission from ref 65. Copyright 2016, Springer Nature. **(d)** The schematic of growth mechanism of well-aligned FF nanotubes. **(e)** Piezoresponses of nanotube film characterized by PFM. **(f)** Power output of fabricated energy harvester as a function of load resistance Reprinted with permission from ref 163. Copyright 2018, the American Chemical Society.

Figure 11.
(a) The schematic fabrication and structural modulation of phage nanopillars. **(b)** The schematics of as-fabricated energy harvester **(c)** Output voltage and current as a function of load resistance. Reprinted with permission from ref 135. Copyright 2015, Royal Society of Chemistry. **(d)** The schematic of monolayer growth process of vertically aligned M13 phage. **(e)** The schematic of as fabricated energy harvester. **(f)** comparison of M13 phage films with different processing and modifications. **(g)** The voltage of capacitor charging by M13 phage energy harvester as a function of time. Reprinted with permission from ref 134. Copyright 2019, the American Chemical Society.

Figure 12.
(a) Digital photograph demonstrating the grasping capability of PLLA tweezer controlled by applied voltage. Reprinted with permission from ref 171. Copyright 2005, Taylor & Francis Group. **(b)** Histological images of PLLA nanofibers implanted after 4 weeks and 12 weeks. Reprinted with permission from ref 174. Copyright 2009, the American Chemical Society. **(c)** The schematic (left) and digital image (right) of the implantable biodegradable piezoelectric sensor. **(d)** In vivo pressure sensing of the biodegradable sensor implanted in the abdominal cavity of rat. Reprinted with permission from ref 146. Copyright 2017, National Academy of Sciences. **(e)** Schematic of as-fabricated chitin-based transducer. **(f)** Comparison of Fourier transform (STFT) spectrograms from the original sound source and chitin speaker. Reprinted with permission from ref 93. Copyright 2018, Elsevier.